

Lawrence Berkeley National Laboratory

Recent Work

Title

THE HEW SPECTROSCOPY

Permalink

<https://escholarship.org/uc/item/89r7x9jv>

Author

Trilling, George H.

Publication Date

1975-10-01

DISCLAIMER

This document was prepared as an account of work sponsored by the United States Government. While this document is believed to contain correct information, neither the United States Government nor any agency thereof, nor the Regents of the University of California, nor any of their employees, makes any warranty, express or implied, or assumes any legal responsibility for the accuracy, completeness, or usefulness of any information, apparatus, product, or process disclosed, or represents that its use would not infringe privately owned rights. Reference herein to any specific commercial product, process, or service by its trade name, trademark, manufacturer, or otherwise, does not necessarily constitute or imply its endorsement, recommendation, or favoring by the United States Government or any agency thereof, or the Regents of the University of California. The views and opinions of authors expressed herein do not necessarily state or reflect those of the United States Government or any agency thereof or the Regents of the University of California.

THE NEW SPECTROSCOPY

George H. Trilling

Department of Physics and Lawrence Berkeley Laboratory
University of California, Berkeley, California 94720

I. THE COMING OF THE NEW SPECTROSCOPY

A. Introductory Remarks

My task in these three lectures is to review the experimental status of the new spectroscopy thrust upon the physics world by the particle discoveries of last fall. Before embarking on this discussion I want to make a few qualifying remarks:

(1) In so rapidly varying a field, the distinction between review lecture and topical seminar becomes blurred. Hence there may be some overlap between material presented here and subjects discussed in more detail in the Topical Conference. I have endeavored not to dwell on those areas which are on the program of the Topical Conference.

(2) By the force of circumstances I have had better access to the pre-publication results of the SLAC-LBL Collaboration than to the work of other groups or laboratories. Thus although I have attempted to take account of all contributions to this field, my presentation may not be as completely balanced as might be desirable.

(3) In the matter of notation I have used the symbols $\psi(3095)$ and $\psi(3684)$ for the two narrow states which are presently the best-established citizens of the new spectroscopy.

(4) I have not discussed in any great detail theoretical models of the new particles except insofar as they bear directly on the interpretation of experimental results. Undoubtedly this important area will receive more emphasis in Haim Harari's subsequent lectures.

B. The "Old" Spectroscopy

The spectroscopy of meson and baryon states was perhaps the major focus of attention for high energy physicists during the decade of the

1960's. The experimental consequence of this effort was the discovery and determination of the properties and quantum numbers of a large number of such states, and the recognition of certain regularities exhibited by these states. While this is not the place to go into any detailed discussion of this subject it may be useful to summarize some basic features of the spectroscopy:

1. There are families of meson and baryon states or resonances. Individual states have been mostly identified in the mass region below 2 GeV. Above that mass, typical resonance widths tend to become larger than level spacings, and structure is much more difficult to recognize. The occurrences of large widths for high-mass states are easy to understand in terms of the large numbers of available decay channels.

2. $SU(2)$ is an exact symmetry of the strong interactions, and $SU(3)$ is an approximate symmetry. Baryons fit into 10, 8, 1 representations and mesons into 8, 1 representations of $SU(3)$. Typical $SU(3)$ -violating mass differences observed within given unitary multiplets amount to $\Delta m^2 \sim 0.2 - 0.5 \text{ GeV}^2$ per unit of hypercharge ($Y = B + S$, where $B \equiv$ baryon number, $S \equiv$ strangeness).

3. The pattern of states can be understood in terms of the Quark Model. For this purpose one considers the three basic spin 1/2 quarks (u, d, s) whose properties are given in the first three rows¹ of Table I. It is assumed that baryons and mesons are constructed out of bound states of the form qqq and $q\bar{q}$ respectively, the binding forces being in first-approximation spin and unitary spin invariant (leading to $SU(6)$ symmetry). Higher mass states are then built up out of radial and orbital excitations of these configurations. The resulting spectrum of levels agrees reasonably with experiment, both in the absence of exotics and in the fact that the observed ordering in terms of energy is consistent with the expected excitations. A review of the quark model was given in one of the lectures of this School last year by Gilman,² and I shall not go

into detail here. It is however desirable, because of later application to the new particles, to discuss briefly the mesons in terms of the quarks of Table I. If L is the orbital angular momentum of the $q\bar{q}$ system and S its total spin, the basic properties are:

Angular momentum	$J = \vec{L} + \vec{S} $
Parity	$P = (-1)^{L+1}$
Charge conjugation ³	$C = (-1)^{L+S}$
G parity	$G = C(-1)^I$

The application to the $L = 0$ states is given in Table II.

It is further worth mentioning here that the isoscalar states observed in nature follow the principle suggested by Table II, namely pure $SU(3)$ singlet and octet for $J^{PC} = 0^{-+}$ and mixed $SU(3)$ representations for $J^{PC} = 1^{--}$. Specifically,

$$\eta = \frac{1}{\sqrt{6}} [u\bar{u} + d\bar{d} - 2s\bar{s}] \quad (\text{octet})$$

$$\eta' = \frac{1}{\sqrt{3}} [u\bar{u} + d\bar{d} + s\bar{s}] \quad (\text{singlet})$$

$$\omega = \frac{1}{\sqrt{2}} [u\bar{u} + d\bar{d}] \quad (\text{mixed octet and singlet})$$

$$\phi = s\bar{s}$$

According to the empirical Zweig rule,⁴ those processes whose quark diagrams have both ends of a quark line belonging to the same hadron are substantially inhibited. This principle coupled with the above representation of the ϕ leads to an understanding of its small width for decay into nonstrange particle combinations such as $\rho\pi$. An identical argument can be used, in the $L = 1$ excitations, to account for the inhibition of the f' decay into nonstrange final state particles. Comparison of the $\rho\pi$ width of the ϕ , namely 0.6 MeV, with the $\rho\pi$ width of the A_2 which is 100 MeV suggests a decay inhibition factor of roughly two orders of magnitude for processes suppressed by the Zweig rule.

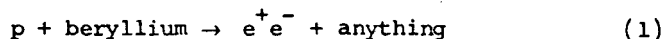
C. The Birth of the New Spectroscopy

The new spectroscopy was introduced to the scientific world in

November 1974. The basic experimental inputs were the following:

(1) The M.I.T.-B.N.L. Experiment⁵

The MIT-BNL group studied the reaction



at a proton energy of 28.5 GeV at the Brookhaven Alternating Gradient Synchrotron (AGS). They used a high-resolution double-arm magnetic spectrometer specifically designed to detect high-mass particles, produced at rest in the center of mass, and decaying into an electron-positron pair. The resulting $e^+ e^-$ mass spectrum,^{6,7} shown in Fig. 1, exhibits an extremely clear resonance at a mass of 3.112 GeV with a width smaller than the experimental resolution, $\Gamma \lesssim 5$ MeV. This particle was given the name J by the MIT-BNL group. Information on its production, as obtained in this experiment, will be discussed in the next lecture. The MIT-BNL group subjected their data to the most careful tests to establish beyond any doubt that the remarkable results shown in Fig. 1 really arose from the decay of a new particle rather than from any non-understood instrumental effect.

(2) The S.L.A.C.-L.B.L. Experiment⁸

The SLAC-LBL group working at the electron-positron storage ring SPEAR at SLAC used a solenoidal magnetic detector to study the reactions



Following up on some unexplained anomalies detected in the course of a systematic study of the energy dependence of the cross section for (2a), they explored during the weekend of November 10, 1974, the cross section behavior for (2a,b,c) in the center-of-mass energy region near 3.1 GeV. The results, which are shown in Fig. 2, exhibit a cross section rise for reaction (2a) of about 100 over the value of about 20 nb observed at 3.0 GeV, accompanied by substantial rises in the cross sections for both (2b)

4a, and the results of its first few hours of operation in a new energy range are shown in Fig. 4b. The evident rise in yield at around 1.85 GeV per beam was subsequently explored in much more detail with the results shown in Fig. 4c. A new resonance, again of width small compared to the machine energy spread, with mass just under 3.7 GeV exhibited itself via a rise of about a factor of 30 in the hadron cross section. Accompanying rises in the dilepton cross sections turn out to be relatively small and were measured accurately only after much more extensive data taking, as will be discussed further. The nomenclature proposed by the SLAC-LBL group for denoting the narrow resonances is $\psi(3095)$ and $\psi(3684)$ (the magnitudes of the mass are recent values revised slightly downward from the original results). I shall use this nomenclature hereafter.

(5) Confirmation of the $\psi(3684)$ at DORIS¹¹

Successful operation of the new e^+e^- storage ring DORIS at the DESY Laboratory permitted the experimental groups there to get quickly into the study of ψ physics. Confirmation of both of the ψ states with the superconducting solenoidal detector PLUTO operating at DORIS is shown in Fig. 5.

Having briefly mentioned the major experiments which detected the existence of the new particles, I just want for completeness to comment on why it was immediately recognized that these new states did not adequately fit into the "old spectroscopy" and required something new. The problem was the understanding of the extraordinarily narrow width, all the more remarkable because the high masses involved, plus the assumed and later verified spin of 1, imply that phase space and angular momentum barrier effects play much less of an inhibiting role than at masses of 1-2 GeV where the usual resonance widths are of the order of 100-300 MeV. The actual ψ widths are 69 and 228 keV respectively for the lower and higher mass states, implying inhibitions of $\sim 10^{-4}$ for hadron decays

and $\sim 10^{-2}$ for first-order electromagnetic decays. It is only the second-order electromagnetic decays (proceeding via the emission and reabsorption of a photon to produce lepton pairs or certain hadron states) which are roughly normal in that their rates are comparable to those of other known vector mesons. Thus the introduction of new quantum numbers or new selection rules to understand these new states seems inevitable.

D. Experimental Techniques of the New Spectroscopy

Much of conventional particle spectroscopy has been carried out with bubble chambers or with fairly straightforward electronic techniques. The new spectroscopy poses serious experimental difficulties because of low cross sections (at least in conventional experiments with hadron or photon beams), and large backgrounds of other processes. Some typical detectors are shown in Figs. 6a, 6b (for fixed target experiments with hadron or photon beams)^{7,12} and Figs. 7a, 7b (for e^+e^- storage ring experiments).^{13,14} The handles used in pursuing such experiments are the following:

- (a) Good effective-mass resolution for two-particle or multiparticle systems to detect narrow bumps (for example, MIT-BNL: $\sigma \approx 5$ MeV).
- (b) Lepton identification capability (MIT-BNL: reject hadrons by 10^8).
- (c) Hadron identification in final state: Cerenkov counters to identify π , K, p for hadron decay modes of interesting states.
- (d) Detection of decays transverse to the beam axis when using hadron collisions as sources of particles. Low-transverse-momentum dominance in hadron processes tends to reduce background.
- (e) Use of e^+e^- storage rings with large-solid-angle detectors. Vector mesons can be directly observed in formation, and their decay modes can be studied effectively. Other states can also be produced in some of the decay modes of the vector mesons.

E. Extraction of Properties of ψ Particles from e^+e^- Storage Ring

Experiments

1. Width of the ψ 's

(a) Basic Formulas

The Breit-Wigner formula for the formation of a resonance of mass M , spin J , width Γ , by e^+e^- collisions of total energy W , in the absence of beam energy spread and radiative corrections, is

$$\sigma_a^R = \frac{(2J+1)\pi}{W^2} \frac{\Gamma_e \Gamma_a}{(W-M)^2 + \frac{\Gamma^2}{4}} \quad (3)$$

where σ_a^R is the cross section, via the resonance, for final state a and Γ_a, Γ_e are the partial widths for decay into state a and into e^+e^- respectively. For a narrow resonance ($\Gamma/M \ll 1$) the cross-section integral over energy is

$$\int \sigma_a^R dW = \frac{2\pi^2}{M^2} (2J+1) \frac{\Gamma_e \Gamma_a}{\Gamma} \quad (4)$$

(b) Beam Energy Spread

Because of the beam energy spread the luminosity (event rate per unit cross section) at a fixed nominal value of the machine total energy W_0 is given to reasonable approximation by

$$\frac{dL}{dW} = f(|W - W_0|) \approx \frac{\mathcal{L}_0}{\sqrt{2\pi} (\Delta W)} \exp\left[-\frac{(W - W_0)^2}{2(\Delta W)^2}\right] \quad (5)$$

where ΔW is the rms energy spread. Although in the neighborhood of a narrow resonance ΔW can be considered constant, it varies with energy roughly as W^2 . In (5) \mathcal{L}_0 is the total machine luminosity at the nominal energy W_0 .

Consider now a very narrow resonance in the sense that $\Gamma \ll \Delta W$. The "effective" cross section $\tilde{\sigma}_a^R$ measured at nominal energy W_0 will be given by,

$$\tilde{\sigma}_a^R \equiv \int \frac{\sigma_a^R(W)}{\mathcal{L}_0} \frac{dL}{dW} dW \Big|_{\text{fixed } W_0} \quad (6)$$

Substituting (5) into (6) we easily find,

$$\tilde{\sigma}_a^R(w_o) = \frac{\sqrt{2\pi^3} (2J+1)}{M^2} \frac{\Gamma_e \Gamma_a}{\Gamma(\Delta W)} \exp\left[-\frac{(M-w_o)^2}{2(\Delta W)^2}\right], \quad (7)$$

and

$$\int \tilde{\sigma}_a^R(w_o) dw_o = \int \sigma_a^R(w) dw = \frac{2\pi^2}{M^2} (2J+1) \frac{\Gamma_e \Gamma_a}{\Gamma}, \quad (8)$$

that is, the cross-section integral is independent of the beam energy spread (the effect of the spread is just to redistribute the events in terms of energy but not to change the cross-section integral).

Note that at the energy corresponding to the peak cross section, $w_o = M$, the ratio of the observed cross section to the true physical cross section in the absence of energy spread is given by

$$\frac{\tilde{\sigma}_a^R(M)}{\sigma_a^R(M)} = \frac{\sqrt{\pi}}{2\sqrt{2}} \frac{\Gamma}{\Delta W}. \quad (9)$$

Thus the measurement of $\tilde{\sigma}_a^R(M)$ (about 2300 nb for hadrons at $\psi(3095)$ according to Fig. 2) does not give a physical result of direct interest but rather one which depends on the energy spread. It is actually the integral (8) which is of direct physical significance. If we wish to deduce the interesting properties Γ and Γ_e from the measurements we can obtain them from (8):

$$\Gamma_e = \frac{M^2}{2\pi^2(2J+1)} \int \tilde{\sigma}_{all}^R(w_o) dw_o \quad (10a)$$

$$\Gamma \equiv \frac{\Gamma_e}{B_e} = \Gamma_e \frac{\int \tilde{\sigma}_{all}^R(w_o) dw_o}{\int \tilde{\sigma}_e^R(w_o) dw_o} \quad (10b)$$

where B_e is the branching ratio for decay into e^+e^- .

One practical difficulty in the implementation of (10) comes from the possibility of completely undetected ψ decay modes (an extreme example would be $\nu\bar{\nu}$) which would lead to an underestimate of $\tilde{\sigma}_{all}^R$. If the branching ratio for such totally undetected modes is given by B_n , the values of Γ_e, Γ determined from (10) neglecting such decay modes

would differ from the true values Γ_e^{true} , Γ^{true} by the factors:

$$\Gamma_e / \Gamma_e^{\text{true}} = 1 - B_n \quad (11a)$$

$$\Gamma / \Gamma^{\text{true}} = (1 - B_n)^2 \quad (11b)$$

There is at present no evidence for any substantial contribution from undetected modes. In the case of the analysis of data from the SLAC-LBL detector, all-photon decay events would be included in the undetected category. Limits from $\gamma\gamma$ and more complicated multi- γ configurations, as shown in Fig. 8 from experiments at DORIS¹⁵ and SPEAR¹⁶ indicate no substantial contribution at the $\psi(3095)$. Thus for purposes of width determination it has been assumed that $B_n \approx 0$.

(c) Radiative Corrections

The formulas so far presented neglect an important factor in the interpretation of the data, namely the radiative corrections. This is a somewhat technical subject and, rather than discussing it in detail, we refer the reader to useful references where the appropriate formulas are given.¹⁷ It may be useful however to mention here that, to correct for radiative effects, one can replace the cross section integral as used in formulas (8) and (10) by,

$$\int \tilde{\sigma}^R dW_0 \rightarrow (W_{\text{max}} \xrightarrow{\text{lim}} \infty) \left[\frac{M}{2(W_{\text{max}} - M)} \right]^t \int^{W_{\text{max}}} \tilde{\sigma}^R dW_0 \quad (12)$$

where

$$t = \frac{2\alpha}{\pi} \left[2 \ln \frac{M}{m_e} - 1 \right] \approx 0.076 \quad \text{for } M = 3.095 \text{ GeV}.$$

Thus the cross-section integral actually diverges, but multiplication by the corrective factor on the right side of (12) gives it a limiting value.

It is worth noting that the radiative effects reduce the peak cross section from the value (9) by approximately the factor

$$\left(\frac{2\Delta W}{M} \right)^t \approx 0.6,$$

a very substantial change.

(d) Experimental Results

The experimental results for the energy dependence of the hadron

and dilepton cross sections in the neighborhood of the two ψ resonances, obtained by the SLAC-LBL group,^{18,19} are shown in Figs. 9 and 10. It should be noted that the hadron cross sections are corrected for the finite acceptance of the detector whereas the dilepton cross sections apply only to an angular region well within the detector acceptance, namely $|\cos \theta| \leq 0.6$ where θ is the angle between either lepton and the incident beam. This procedure is followed because the acceptance corrections for multihadron events, in which the multiplicities are relatively large and the particles are emitted isotropically, are independent of spin-parity assignment, whereas the angular distributions of the dilepton events are sensitive to this spin assignment. It will be shown that the correct assignment for both ψ 's is $J = 1$, from which the dilepton angular distribution is $1 + \cos^2 \theta$, and the resonance parts of the cross sections shown in Fig. 9b,c and 10b,c are 50% of the actual resonance dilepton cross sections. One other important remark is that the large background under the cross sections for the e^+e^- final states arises from the t-channel scattering diagram (Rutherford scattering) which is of course absent for the $\mu^+\mu^-$ final state. This nonresonant contribution to the e^+e^- scattering peaks at small angles, and is used to determine the luminosity of the machine.

The widths and branching ratios Γ , Γ_e , Γ_μ , B_e , B_μ for the $\psi(3095)$ have been determined from the data shown in Fig. 9, using a slightly more sophisticated version of the formulas given in the previous sections and are shown in Table III, together with corresponding results from the Frascati group.²⁰ There is remarkably good agreement, considering the estimated errors (which arise principally from the systematics of determining detection efficiencies for multihadron events). Furthermore the quoted parameters also agree well with determinations of the combinations $\Gamma_e \Gamma_\mu / \Gamma$, Γ_e^2 / Γ from cross sections for e^+e^- and $\mu^+\mu^-$ final states [see Eq. (4)] as measured by the DESY-DASP¹³ and SPEAR-HEPL groups.¹⁶ The

corresponding properties for the $\psi(3684)$ as determined from Fig. 10 by the SLAC-LBL group¹⁹ are given in Table IV. In addition to the usual widths, masses and branching ratios, Table III and IV contain the quantities, J^{PC} and $\Gamma_{\gamma h}$. The determinations of J^{PC} will be discussed in the next section, and we define $\Gamma_{\gamma h}$ in the following paragraph.

The quantity $\Gamma_{\gamma h}$ represents that part of the ψ decay width into hadrons which proceeds via an intermediate photon (second-order electromagnetic process, Fig. 11b), rather than directly (Fig. 11a). To obtain it one assumes that ψ decay into dimuons also proceeds via an intermediate photon (Fig. 11d) and that the corresponding ratio of hadron to dimuon production is the same on resonance as it is in a neighboring energy range off resonance (Fig. 11c,e):

$$\Gamma_{\gamma h} = \Gamma_{\mu} \left[\frac{\sigma[e^+e^- \rightarrow \text{hadrons}]}{\sigma[e^+e^- \rightarrow \mu^+\mu^-]} \right]_{\text{off resonance}} \quad (13)$$

The ratio in brackets, commonly given the symbol R , is of great interest in its own right and has been measured over the SPEAR energy range by the SLAC-LBL group.²¹ The published values were used in (13) to determine the values of $\Gamma_{\gamma h}$. In so doing, interference effects between second-order electromagnetic and direct decays have been neglected.

It is interesting to compare from Tables III and IV the properties of the $\psi(3684)$ relative to those of the $\psi(3095)$. The total width is about a factor of three larger, the leptonic widths are about half as large, and the leptonic branching ratio is down by a factor of seven. This circumstance helps make the $\psi(3684)$ relatively difficult to detect in processes other than annihilation. As will be discussed later, the hadronic decay processes of the $\psi(3684)$ are remarkably different from those of the $\psi(3095)$.

2. Determination of J^{PC}

(a) Basic Considerations

The leptonic decay widths of the $\psi(3095)$ and $\psi(3684)$ are comparable to those of the well-known vector mesons produced in annihilation,

namely ρ , ω , ϕ . This suggests that the ψ 's are also vector mesons with the quantum numbers of the photon, but evidently this hypothesis requires experimental verification. As a first step we examine in Fig. 12 the forward-backward asymmetry in dimuon production in narrow energy regions spanning the two ψ resonances. There is no significant asymmetry as expected from the decay of a state of definite parity. Indeed, even in the region a few MeV below the resonance where maximal interference between the QED amplitude and the ψ decay amplitude can be expected to occur (see discussion further on) there is no evidence of an asymmetry, suggesting the same parity for the photon and the ψ .

The most compelling way to check if the ψ and the photon have the same quantum numbers is to search for interference effects in the energy dependence of the cross section for dimuon production in the neighborhood of the resonance energy. Consider first an ideal 4π detector and let A_γ , A_ψ represent amplitudes for annihilation into two muons via an intermediate photon (QED amplitude) and an intermediate ψ , respectively (see Figs. 11e and 11d). The $\mu^+\mu^-$ final state has been chosen because the QED amplitude is well understood, the ψ 's decay into it, and there is no t-channel contribution (as in e^+e^-) which would mostly add noise rather than signal. Assuming μ -e universality [supported by the measured equality of Γ_e and Γ_μ for the $\psi(3095)$] the resonant Breit-Wigner amplitude A_ψ is just the elastic amplitude and will be positive real for $W < M$, and negative real for $W > M$. The QED amplitude is similarly negative real (as expected if one thinks of the photon as equivalent to a zero mass resonance). Thus one would expect, if the ψ has the quantum numbers of a photon, destructive interference below the resonance and constructive above. Because of the complications of the radiative tail for $W > M$ as well as the fact that destructive interference is generally easier to detect, it is the region below the resonance which is most useful for this study.

The relevant cross sections for $|W - M| \gg \Gamma$ are

$$|A_\gamma|^2 = \sigma_{\mu\mu}^\gamma = \frac{4\pi}{3} \frac{\alpha^2}{W^2} \quad (14a)$$

$$|A_\psi|^2 = \sigma_{\mu\mu}^\psi = \frac{3\pi}{W^2} \frac{\Gamma_e^2}{(W - M)^2} \quad (14b)$$

assuming here that $J = 1$. Thus if the γ and ψ have the same quantum numbers, there will be complete destructive interference when $|A_\gamma|^2 = |A_\psi|^2$ or

$$M - W = \frac{3\Gamma_e}{2\alpha} \approx \begin{array}{ll} 1 \text{ MeV} & \psi(3095) \\ 0.5 \text{ MeV} & \psi(3684) \end{array} \quad (15)$$

This argument has so far neglected the energy spread in the storage ring, whose standard deviation ΔW is of the order of 1-2 MeV, depending on which ψ is being studied. It is evident therefore that if one sits at a nominal energy W_0 1 MeV below the resonance, as suggested by (15), a sizable fraction of the beam will still be at the peak of the resonance and it will be impossible to detect destructive interference. However, as long as ΔW is not large compared to

$$\frac{3}{2} \frac{\Gamma_e}{\alpha} \quad (16)$$

it is perfectly possible to go to energies a little further below the resonance, obtaining partial but not complete destructive interference and getting even the tails of the beam energy distribution away from the resonance peak. In practice it is most convenient to calculate, taking the energy spread into account, the expected values of the ratio $\sigma_{\mu\mu}/\sigma_{ee}$ as a function of the nominal energy W_0 , with and without interference, and compare them with experiment. The results as obtained by the SLAC-LBL group^{18,19} are shown in Figs. 13a and 13b. They provide conclusive evidence for destructive interference between the QED and resonance amplitudes below resonance for both $\psi(3095)$ and $\psi(3684)$.

(b) Effect of Detector Solid Angle

The above result of destructive interference between the QED and resonance amplitudes provides an unambiguous determination of the ψ

quantum numbers if the detector subtends with uniform efficiency the complete solid angle.

The real detector used at SPEAR however can be considered as fully efficient only over the more restricted angular range,

$$-0.6 \leq \cos \theta \leq 0.6 \quad \text{and} \quad 0 \leq \varphi \leq 2\pi$$

where θ , φ are polar and azimuthal angles relative to the beam direction.

From this one can deduce the following:

(1) Since the detector is symmetric in $\cos \theta$, the observed interference implies equal parities for the ψ and the photon, both negative.

(2) Since the detector is equally sensitive to negative and positive particles within its acceptance solid angle, the interference implies equal values of the charge conjugation quantum number for the photon and the ψ , namely $C = -1$.

(3) However, the observation of interference does not, without further argument, rule out $J_\psi \neq 1$.

We consider this question in more detail. Let $A(\vec{P}, m, \lambda_+, \lambda_-)$ be the amplitude for producing a $\mu^+ \mu^-$ in the direction \vec{P} (angles θ, φ) with helicities λ_+, λ_- if m is the spin projection of the initial γ or ψ along the beam axis. Then we can write,^{22,23}

$$A(\vec{P}, m, \lambda_+, \lambda_-) = f(m, \lambda_+, \lambda_-) d_{m\Lambda}^J(\theta) e^{i\varphi(m-\Lambda)} \quad (17)$$

where $\Lambda = \lambda_+ - \lambda_-$. Furthermore we can apply the following conditions:

(i) Parity conservation

$$f(-m, -\lambda_+, -\lambda_-) = f(m, \lambda_+, \lambda_-) \quad (18a)$$

(ii) Definite parity η of the intermediate state ($\eta_\gamma = -1$ for photons, $\eta_\psi = -1$ for ψ)

$$\begin{aligned} f(m, -\lambda_+, -\lambda_-) &= \eta(-1)^J f(m, \lambda_+, \lambda_-) \\ &= (-1)^{J+1} f(m, \lambda_+, \lambda_-) \end{aligned} \quad (18b)$$

(iii) Neglecting terms of order m_e/M , m_μ/M , the QED amplitude is nonvanishing only for $m = \pm 1$, $\Lambda = \pm 1$.

It follows that the angular distribution is given by

$$F(\theta) = \sum_{\substack{m=\pm 1 \\ \Lambda=\pm 1}} [f^{\psi(m, \lambda_+, \lambda_-)} d_{m\Lambda}^J(\theta) + f^{\gamma(m, \lambda_+, \lambda_-)} d_{m\Lambda}^1(\theta)]^2. \quad (19)$$

Using (18) and the properties of the $d_{m\Lambda}^J$ functions,

$$d_{-1-1}^J = d_{11}^J; \quad d_{-11}^J = d_{1-1}^J; \quad d_{-11}^J(\theta) = (-1)^{J+1} d_{11}^J(\pi - \theta) \quad (20)$$

we can finally write,

$$F(\theta) = 2[f^{\psi(1, 1/2, -1/2)} d_{11}^J(\theta) + f^{\gamma(1, 1/2, -1/2)} d_{11}^1(\theta)]^2 + 2[f^{\psi(1, 1/2, -1/2)} d_{11}^J(\pi - \theta) + f^{\gamma(1, 1/2, -1/2)} d_{11}^1(\pi - \theta)]^2. \quad (21)$$

From (21) we can immediately calculate the ratio of interference for any value of J relative to that for $J = 1$ integrated over the detector:

$$\text{Interference Ratio} = \frac{\int_{-0.6}^{0.6} d_{11}^J(\theta) d_{11}^1(\theta) d \cos \theta}{\int_{-0.6}^{0.6} d_{11}^1(\theta) d_{11}^1(\theta) d \cos \theta}. \quad (22)$$

The results of such calculations can be summarized as follows:

<u>J-Value</u>	<u>Interference Ratio</u>	<u>Interference (W < M)</u>
0	0	0
1	1	large destructive
2	negative	constructive
3	negative	constructive
> 3	very small	very small

Thus, even considering the finite size of the SLAC-LBL detector, one still concludes that the observed interference demonstrates that $J^{PC} = 1^{--}$ for both the $\psi(3095)$ and the $\psi(3684)$.

Finally, from (21) with $J = 1$, we easily obtain the expected dilepton angular distribution for the ψ 's:

$$F(\theta) \sim [d_{11}^1(\theta)]^2 + [d_{11}^1(\pi - \theta)]^2 \sim 1 + \cos^2 \theta. \quad (23)$$

Comparison with experiment is shown in Fig. 14 and is satisfactory.

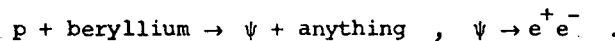
II. THE HADRONIC PROPERTIES OF THE ψ 'S

A. Production of ψ in Hadronic Reactions

We summarize data on the production of ψ in hadron-initiated processes by listing and discussing the various relevant experiments. As of now, the statistics in most of these experiments are still relatively sparse, but one may, in the next year or two, expect dramatic improvements and considerably more refined results.

(1) The M.I.T.-B.N.L. Experiment^{6,7}

This experiment has already received some discussion in the previous lecture since it provided the very first observation of the $\psi(3095)$. It utilized a spectrometer (Fig. 6a) specifically designed to look for production with center-of-mass momentum $P^* \approx 0$, in the reaction,



To transform observations in such a limited region of phase space to a cross section for ψ production, one needs a production model, which the MIT-BNL group took to be

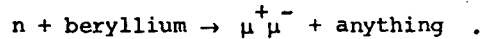
$$\frac{d^3\sigma}{dP_{\parallel}^* dP_{\perp}^{*2}} \sim \frac{e^{-6P_{\perp}^*}}{E^*} .$$

With the $e^+ e^-$ branching ratio given in Table III, the MIT-BNL group estimates a $\psi(3095)$ production cross section at 28.5 GeV incident proton energy of about 1.4 nb/nucleon. At 20 GeV incident energy, the cross section is down by a factor of about 10. Finally, going back to 28.5 GeV, there was no observation of $\psi(3684)$ production yielding an upper limit of 0.1 nb/nucleon for its cross section (due account being taken of the $e^+ e^-$ branching ratio given in Table IV).

(2) The Columbia-Cornell-Hawaii-Illinois-FNAL Experiment²⁴

The CCHF experiment was set up in a neutral beam at the Fermilab. A 34-meter liquid deuterium tube could be used to attenuate neutrons and produce a highly enriched photon beam for photoproduction experiments; or, alternatively the deuterium was removed, and a 3.8-cm lead absorber was

used to remove photons and produce an almost pure neutron beam. The neutron energy spectrum, monitored with a calorimeter, peaked at around 250 GeV. The reaction studied with an absorber and magnetic spectrometer (Fig. 6b) is:



The dimuon mass spectrum obtained, shown in Fig. 15 shows in addition to the large expected ρ peak a clear structure at around 3.1 GeV, with a width compatible with the rather poor resolution (poor because of the large absorber traversal of the muons prior to analysis in the spectrometer). The corresponding cross section, estimated to within a factor of 2, for production of $\psi(3095)$ is given as follows

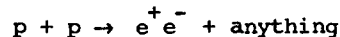
$$\sigma \approx 24 \text{ nb/nucleon for } |x| > 0.32$$

$$\sigma \approx 50 \text{ nb/nucleon for } |x| > 0.24$$

where $x = \frac{\psi \text{ momentum}}{\text{neutron momentum}}$ and again correction has been made for the dimuon branching ratio. It seems clear from these numbers that after extrapolation to $|x| = 0$ the cross section will be of order 10^2 nb/nucleon, and hence about two orders of magnitude larger than at 28.5 GeV.

(3) The CERN-Columbia-Rockefeller-Saclay Experiment²⁵

The CCRS experiment detected at the CERN Intersecting Storage Rings the reaction



for a range of equivalent proton laboratory energies extending from 500 to 2000 GeV, in the neighborhood of $P^* = 0$. The observed $e^+ e^-$ invariant mass distribution, shown in Fig. 16, shows a small but significant contribution in the neighborhood of 3.1 GeV. The cross section, corrected for the $e^+ e^-$ branching ratio, is estimated to be

$$\frac{d\sigma}{dy} \approx (100 \pm 30) \text{ nb}$$

where y is the rapidity and the cross section is averaged over the c.m. rapidity interval $-0.32 < y < +0.32$. Integrating over rapidities gives

a cross section of order 10^2 nb which is comparable to the result from 250 GeV neutrons at Fermilab. It is worth noting that the observed ψ cross section falls by about an order of magnitude to account for the direct lepton production observed in the ISR experiment.

(4) The Northeastern Experiment²⁶

The Northeastern group has reported the results of a comparison of the reactions

$$\pi^- + \text{iron} \rightarrow \mu^+ \mu^- + \text{anything}$$

$$p + \text{iron} \rightarrow \mu^+ \mu^- + \text{anything}$$

with the dimuons in the mass region of the $\psi(3095)$ where a small but significant signal is detected. The x and P_{\perp} distributions for incident protons and pions shown in Fig. 17 are parametrized in the following way:

$$\frac{d^3\sigma}{dx dP_{\perp}^2} \propto e^{-ax - bP_{\perp}}$$

$$a_p = 9.7 \pm 1.6$$

$$a_{\pi} = 6.2 \pm 0.8$$

$$b_p = 2.2 \pm 0.5 \text{ GeV}^{-1}$$

$$b_{\pi} = 1.6 \pm 0.2 \text{ GeV}^{-1}$$

and

$$\frac{(\text{yield})_{\pi}}{(\text{yield})_p} = 7.4 \pm 2.0 \quad \text{for } |x| \geq 0.5$$

Thus the center-of-mass longitudinal momentum spectrum falls off more rapidly for incident protons than for incident pions. The large yield from incident pions relative to incident protons at large $|x|$ seems to reflect this difference in fall-off. Indeed if one extrapolates to $x = 0$ the total cross section for $\psi(3095)$ production from incident pions appears comparable to that from incident protons.

We can summarize the results of experiments in which ψ mesons are produced by hadron beams:

- (i) Only cross sections for $\psi(3095)$ have been measured. The hadronic production of $\psi(3684)$ has not at this time been reported. This presumably reflects both low cross sections and the small branching ratio of $\psi(3684)$ into dileptons.

(ii) $\psi(3095)$ production cross sections rise from about 1 nb at 30 GeV to hundreds of nb at energies of 200 GeV up to 2000 GeV. There appears to be no dramatic increase in production cross section between 200 and 2000 GeV.

(iii) $\psi(3095)$ production by incident pions is comparable to production by incident protons but is less confined to small longitudinal center-of-mass momenta.

(iv) Transverse momentum distributions of ψ appear to be broader than those of lower mass hadrons, such as pions or ρ .

B. Photoproduction of ψ

1. Basic Relations²⁷

We start with two basic relations:

(a) Coupling constant of vector meson to virtual photon from its leptonic width,

$$\frac{\gamma_V^2}{4\pi} = \frac{\alpha^2}{12} \frac{M_V}{\Gamma_{\text{lepton}}} \quad (24)$$

(b) Vector meson dominance,

$$\sigma(\gamma + A \rightarrow B + C) = \sum_V \frac{\alpha\pi}{\gamma_V^2} \sigma(V + A \rightarrow B + C) \quad (25)$$

If we let B be a particular vector meson and neglect processes $V + N \rightarrow V' + N$, V and V' being different vector mesons, we obtain from (25),

$$\frac{d\sigma}{dt}(\gamma + N \rightarrow V + N) = \frac{\alpha\pi}{\gamma_V^2} \frac{d\sigma}{dt}(V + N \rightarrow V + N) \quad (26)$$

Finally if we apply the optical theorem and neglect the real part of the forward $V + N$ amplitude, we find easily from (26)

$$\left. \frac{d\sigma}{dt} \right|_{t=0}(\gamma + N \rightarrow V + N) = \frac{\alpha}{64\pi} \frac{[\sigma_{\text{tot}}(VN)]^2}{(\gamma_V^2/4\pi)} \quad (27)$$

The values of $\gamma_V^2/4\pi$ for the $\psi(3095)$ and $\psi(3684)$ can be evaluated from (24) to be 2.86 ± 0.36 and 7.4 ± 1.1 using results from Table III and IV. If one assumes that the same value of γ_V^2 can be used in (27) as in (24)

(note that there is a difference in the mass-squared of the photon of $\sim 10 \text{ GeV}^2$), then an experimental determination of the forward ψ diffractive photoproduction cross section will immediately yield, via (27), an estimate of $\sigma_{\text{tot}}(\psi N)$. This, in turn, can help establish the hadronic character of the ψ . We now consider the experimental results.

2. Experimental Results on ψ Photoproduction

Measurements of ψ photoproduction have been reported by three groups:

- (a) Cornell Group²⁸: $\gamma + \text{Be}$ at 11.8 GeV,
- (b) SLAC-Wisconsin Group²⁹: $\gamma + \text{D}_2$ and $\gamma + \text{H}_2$ at 13-21 GeV,
- (c) Columbia-Cornell-Hawaii-Illinois-FNAL Group¹²: $\gamma + \text{Be}$ at 100-200 GeV.

Figures 18 and 19 show some data from the Cornell and CCHIF experiments and Fig. 20 (put together by the Cornell group) summarizes the energy dependence of the forward photoproduction cross section for $\psi(3095)$ using data from all three experiments. The results from these experiments can be summarized as follows:

(i) The process $\gamma N \rightarrow \psi(3095)N$ occurs with a cross section which is measurable by these experiments. Indeed Fig. 19 shows clearly the coherent diffractive photoproduction of $\psi(3095)$ by beryllium nuclei.

(ii) The SLAC-Wisconsin experiment has, at its highest energy of 21 GeV, observed production of both $\psi(3095)$ and $\psi(3684)$, with a ratio $\psi(3095)/\psi(3684)$ at t_{min} of 6.8 ± 2.4 . The CCHIF also has a few $\psi(3684)$ events, but no cross section for these has been reported.

(iii) Both $\left. \frac{d\sigma}{dt} \right|_{t=0}(\gamma N \rightarrow \psi(3095)N)$ and the slope increase with energy over the total energy range covered (slope goes from 1.2 GeV^{-2} at 11.8 GeV to about 4 GeV^{-2} at 100 GeV).

(iv) From Eq. (27), with γ_V^2 determined from Γ_e using (24), the highest energy data lead to $\sigma_{\text{tot}}[\psi(3095)N] \approx 1 \text{ mb}$. Although this cross section is relatively small, as compared to the cross sections for other vector mesons, it seems sufficiently large to support the interpretation of the $\psi(3095)$ as a hadron.¹²

C. Hadronic Decay Modes of $\psi(3095)$

1. General Considerations

Table V gives a summary of present information on $\psi(3095)$ hadronic decay modes based on the experimental results of the SLAC-LBL group³⁰ and the DESY-DASP group.³¹ The SLAC-LBL group has, in a further analysis, addressed the question of whether the usual strong interaction symmetries SU(2) and SU(3) are applicable to these hadronic decays. To do this, one identifies those final states which have a large "direct" contribution (see Fig. 11a) as opposed to states whose branching ratios can be accounted for by second-order electromagnetic processes (see Fig. 11b), and which only contribute to the width $\Gamma_{\gamma h}$ defined by Eq. (13). If the $\psi(3095)$ is a state of definite isospin (as expected if it is a hadron), and if isospin is conserved in its direct decays, the decay modes so produced should be states of definite isospin I and G parity, the two being related in the usual way,

$$G = C(-1)^I = (-1)^{I+1} . \quad (28)$$

To test specifically whether a particular decay mode "a" has a substantial direct contribution, one defines the cross-section ratio,

$$\alpha_a \equiv \left[\frac{\sigma_a(3095)}{\sigma_{\mu\mu}(3095)} \right] \left[\frac{\sigma_{\mu\mu}(3000)}{\sigma_a(3000)} \right] \quad (29)$$

where $\sigma(3000)$ represents a cross section at $W = 3000$ MeV, just below the mass of the $\psi(3095)$, where substantial data are available from earlier running at SPEAR. If $\alpha_a \approx 1$, the decay mode "a" can be accounted for by a second-order electromagnetic transition, whereas if $\alpha_a \gg 1$, the decay is bound to have a substantial direct component. We now discuss the results of applying this procedure.

2. G-Parity of $\psi(3095)$

Consider as an example events in which four charged prongs of total charge zero are detected. The missing-mass-squared distribution for events with missing momentum > 0.2 GeV/c (to ensure that there is a missing neutral) are shown in Fig. 21a ($W = 3000$ MeV) and Fig. 21b

($W = 3095$ MeV). The resonance data indicates a substantial contribution from the final state $2\pi^+2\pi^-X$ where X is a low-mass object which we tentatively identify as a π^0 . This identification will be discussed in more detail further on. The absence of a corresponding signal in Fig. 21a then suggests that the decay mode $2\pi^+2\pi^-\pi^0$ is a direct one.

Figure 22 summarizes the results of determinations of the ratio α for various pion multiplicities consisting of one or zero neutral pions plus an even number of pions of total charge zero, identified in the manner illustrated in Fig. 21. The remarkable result is that $\alpha \approx 1$ for even multiplicities and $\alpha \gg 1$ for odd multiplicities. The natural interpretation of this result is that the $\psi(3095)$ is a hadron state of odd G-parity and, from (28), even isotopic spin, and that the direct hadronic decay modes are isospin-conserving.

3. Isotopic Spin of the $\psi(3095)$

(i) $\pi^+\pi^-\pi^0$ decay mode:

The Dalitz plot for the $\pi^+\pi^-\pi^0$ decay mode,³⁰ shown in Fig. 23, exhibits very strong dominance by the quasi-two-body final state $\rho\pi$. Furthermore it is clear that the three charge states $\rho^+\pi^-$, $\rho^-\pi^+$ and $\rho^0\pi^0$ populate the Dalitz plot in roughly comparable numbers. Taking account of detection efficiencies, one finds

$$\frac{\Gamma(\rho^0\pi^0)}{\Gamma(\rho^+\pi^- + \rho^-\pi^+)} = 0.59 \pm 0.17 ,$$

to be compared with the predicted values of 0.5 and 2.0 for isospins zero and two respectively, these being the only isospins permitted by the odd G parity. Obviously the isospin value of zero is established.

(ii) $\bar{\Lambda}\Lambda$ decay mode:

The $\bar{\Lambda}\Lambda$ decay mode has been identified by the SLAC-LBL group from a study of decay modes of the form $p\bar{p}\pi^+\pi^-$ in which p and \bar{p} are recognized by time-of-flight.³² Figure 24 shows a scatter plot of the momentum of the Λ vs the momentum of the $\bar{\Lambda}$ with a clear cluster at 1080 MeV/c for both momenta, the value corresponding to the $\bar{\Lambda}\Lambda$ decay of the $\psi(3095)$.

Since the $\bar{\Lambda}\bar{\Lambda}$ system can only have isospin zero, the only further point which needs consideration is whether this decay mode is indeed a direct one. The procedure of comparison with data at 3000 MeV is not useful here because of the small cross section involved. However Gilman³³ has pointed out that from an SU(3) argument, one expects for states produced via an intermediate photon,

$$\frac{\Gamma(\bar{\Sigma}^0\bar{\Lambda} + \bar{\Sigma}^+\bar{\Lambda}^-)}{\Gamma(\bar{\Lambda}\bar{\Lambda})} = 6/1 .$$

In fact, with 20 $\bar{\Lambda}\bar{\Lambda}$ events detected no clear-cut $\bar{\Sigma}^0\bar{\Lambda}$, $\bar{\Sigma}^+\bar{\Lambda}^-$ events have been observed and the above ratio is less than 1/1, and hence far from 6/1. It follows that the $\bar{\Lambda}\bar{\Lambda}$ decay is direct, and the $\psi(3095)$ isospin is zero.

(iii) $p\bar{p}$ decay mode:

Both the DESY-DASP and the SLAC-LBL groups have detected the decay mode $p\bar{p}$ with branching ratio $\sim 0.2\%$ (see Table V). As pointed out by the DESY-DASP group,³¹ this branching ratio is far too large to be accounted for via a second-order electromagnetic process, using any reasonable form factor and extrapolating from lower energy observations. Hence the observed $p\bar{p}$ decay must be direct. Its isospin can only be zero or one, and since the latter is excluded by the G-parity analysis, the isospin must be zero.

4. What about decay modes with the direct emission of a photon?

Certain classes of models, namely those which involve the quantum number of color, predict that the dominant decay modes of the $\psi(3095)$ are of the form,

$$\psi(3095) \rightarrow \text{hadrons} + \gamma . \quad (30)$$

The dominance of such decay modes could provide an alternative interpretation of Fig. 22 if the missing neutral particle were in fact a photon rather than a π^0 . Although for individual events with a low-mass missing neutral, the distinction between a γ and a π^0 is often impossible to make, the totality of the data fit far more naturally to a missing π^0 hypothesis

than to a missing photon hypothesis, as is clear from the following arguments:

(i) The resolution in missing-mass-squared is roughly proportional to the momentum of the missing neutral. Thus for low-momentum neutrals the resolution is very good and clearly fits the missing π^0 and not the missing γ hypothesis. Even from study of the average of all events in Fig. 21b, it is clear that the average missing-mass-squared fits much better to 0.02 GeV^2 than to zero.

(ii) A clear ω signal (see Fig. 25) is observed in the $\pi^+ \pi^- \pi^0$ effective mass for the $\pi^+ \pi^- \pi^+ \pi^- \pi^0$ final state. For those events, which amount to about 20% of the total, the missing neutral is clearly a π^0 .

(iii) The decomposition of the $\pi^+ \pi^- \pi^0$ final state into equal amounts of $\rho^+ \pi^-$, $\rho^- \pi^+$ and $\rho^0 \pi^0$ is easily interpretable only if the missing neutral is a π^0 .

Thus while the existence at some level of decay modes of the form (30) can certainly not be ruled out by the data, it is very unlikely that they account for any substantial fraction of $\psi(3095)$ decays, as predicted by color models.

5. What about interference effects?

In the analysis of the G-parity, we have not considered the effects of interference between direct and second-order electromagnetic decays. It is however a feature of the multipion final states that the electromagnetic decays are dominated by isovector amplitudes and even G-parity, whereas the direct decays exhibit the isoscalar and odd G-parity properties of the $\psi(3095)$. Thus there is almost no overlap between the final states, and interference effects are most likely small.

6. Is the $\psi(3095)$ an SU(3) singlet?

(a) Predicted behavior on singlet hypothesis:

Consider first the decay mode

$$\psi \rightarrow M_1 \bar{M}_2$$

where M_1, M_2 are nonstrange mesons such that the charge conjugation quantum numbers C_1, C_2 of their neutral states are the same; i.e., $C_1 = C_2$. If ψ is a singlet, $I_1 = I_2$, and therefore it follows from (28) that $G_1 = G_2$. Hence $G(\psi) = G_1 G_2 = +1$ which of course is in conflict with the experimental G-parity determination $G = -1$. One concludes that if the ψ is an isospin singlet, the above decay mode is forbidden by isospin conservation. Thus for example the decay modes $\pi^+ \pi^-$ or $\rho^+ \rho^-$ or $\pi \Lambda_2$ are forbidden. Furthermore, since for an SU(3) singlet there is but a single decay amplitude, decay modes into other members of the same octets as the M_1, M_2 mesons above are forbidden by SU(3) symmetry. Thus the decay modes $K^+ K^-$, $K_L^0 K_S^0$, $K^*(890) \bar{K}^*(890)$, $KK^*(1420)$ are forbidden.

Considering now the decay mode

$$\psi \xrightarrow{?} M_1 \bar{M}_2$$

where the only change from above is that $C_1 = -C_2$, one easily sees that such decay modes are allowed for an SU(3) singlet. However there is a definite rate relation, namely that all combinations of members from a given pair of octets are equally probable. Thus, for example, the rates for $\rho^+ \pi^-$, $\rho^0 \pi^0$, $\rho^- \pi^+$, $K^{*+}(890) K^-$, $K^+ K^{*-}(890)$, $K^0 \bar{K}^{*0}(890)$, $\bar{K}^0 K^{*0}(890)$, etc., are all predicted to be equal, except perhaps for small phase space and angular momentum barrier corrections.

(b) Experimental Results:

Table VI summarizes the situation with respect to tests of the SU(3) singlet hypothesis for $\psi(3095)$. The decay modes which are predicted to be absent are indeed not observed although in some cases the upper limits are not terribly small. The ratio $\rho\pi/KK^*(890)$ is about a factor of 3 higher than predicted by the singlet hypothesis, which is substantially more than can easily be accounted for by phase space and angular momentum barrier corrections. The ratio $p\bar{p}/\Lambda\bar{\Lambda}$, which is expected to be unity, seems to satisfy the prediction within the large uncertainties (see Table V). Thus SU(3) symmetry, with the $\psi(3095)$ a singlet, seems approximately satisfied although

there seems to be some breaking in the $\rho\pi$, $K^*(890)K$ final states.

D. Hadronic Decay Modes of $\psi(3684)$

Table VII summarizes present information³⁰ on the decay modes of the $\psi(3684)$. The results can be best summarized as follows:

- (1) The dominant decay mode is the cascade decay³⁴

$$\psi(3684) \rightarrow \psi(3095) + X$$

In about 60% of these cascade decays, the X is a $\pi^+\pi^-$ pair. Except for a small fraction of $\eta \rightarrow \pi^+\pi^-\pi^0$ or $\pi^+\pi^-\gamma$ decays, those states X which are not $\pi^+\pi^-$ consist of only neutral particles, presumably $\pi^0\pi^0$ for the most part.

The data, from the SLAC-LBL group, are shown in Figs. 26 and 27. In Fig. 26, showing for dimuon and dielectron final states the scatter plot of the positive momentum versus the negative momentum, the events lying on the 45° bands arise from cascade decays with X consisting of only neutrals. The fact that these events lie on 45° bands of the form $P_+ + P_- = \text{constant}$ implies that their effective mass is fixed (at 3095 MeV) but their total momentum can vary depending on the mass of X and the decay angles. Figure 27a shows the inclusive $\mu^+\mu^-$ mass spectrum with clear $\psi(3684)$ and $\psi(3095)$ peaks. Figure 27b shows the $\pi^+\pi^-$ missing mass spectrum with the peak giving evidence for the $\pi^+\pi^- \psi(3095)$ final state. Figure 27c is that subset of Fig. 27b corresponding to 4-prong events of zero total charge and, within errors, zero missing momentum. The background-free peak corresponds to decays,

$$\begin{aligned} \psi(3684) &\rightarrow \psi(3095)\pi^+\pi^- \\ &\quad | \rightarrow \mu^+\mu^- \text{ or } e^+e^- . \end{aligned}$$

The ratio,

$$\frac{\Gamma[\psi(3684) \rightarrow \psi(3095) + \text{neutrals}]}{\Gamma[\psi(3684) \rightarrow \psi(3095) + \text{anything}]} \quad (31)$$

has been determined by the SLAC-LBL group to be 0.44 ± 0.03 , the rather small uncertainty reflecting the fact that most systematic errors cancel.

out in the ratio. If we assume that the neutrals consist largely of $\pi^0 \pi^0$ and neglect the $\psi(3095)\eta$ final state, the above ratio is predicted to have a value of 0.33 if the $\pi\pi$ isospin is zero, zero if the $\pi\pi$ isospin is one, and 0.67 if the $\pi\pi$ isospin is two. Taking account that there may be other neutral states than $\pi^0 \pi^0$ (specifically $\eta \rightarrow \gamma\gamma$ and possibly other $\gamma\gamma$ radiative cascades), the $\pi\pi$ isospin zero is strongly preferred, from which it directly follows that the $\psi(3684)$ also has isospin zero.

The most natural assumption for the $\pi\pi$ amplitude in the $\psi(3095)\pi\pi$ decay mode is that it is an S-wave. Preliminary studies of angular distributions are consistent with this assignment. However the $\pi^+ \pi^-$ mass spectrum⁵ shown in Fig. 28, departs substantially from phase space predictions, even modified for final state interactions, in that the low mass population is strongly suppressed. The correct interpretation of this behavior is an open question.

Since the ratio (31) has a value larger than 0.33, the number expected for $\pi^0 \pi^0$ in an isospin zero state, it becomes of interest to get some handle on what the other neutral objects accompanying $\psi(3095)$ might be. In Fig. 29, the mass spectrum of all neutrals recoiling against $\psi(3095)$ is shown. Furthermore subtraction of the expected $\pi^0 \pi^0$ contribution calculated from $\pi^+ \pi^-$ using the isospin zero prediction leads to the shaded population in Fig. 29. Besides a fairly clear η peak, there is a roughly uniform population whose interpretation is at present the subject of considerable study. Of particular interest is the possibility that this decay mode is

$$\psi(3684) \rightarrow \psi(3095) + \gamma_1 + \gamma_2, \quad (32a)$$

where the decay proceeds via an intermediate state,

$$\psi(3684) \rightarrow X + \gamma_1 \quad (32b)$$

which itself then decays,

$$X \rightarrow \psi(3095) + \gamma_2. \quad (32c)$$

This question will be discussed again in the next lecture.

One final remark concerning the cascade mode is important. Considering the available phase space for $\psi(3684) \rightarrow \psi(3095)\pi\pi$ relative to other possible decay modes, one is forced to conclude from the large branching ratio for that mode that it is much less inhibited than other hadron decay modes of either ψ particle. This emphasizes the necessarily close connection which must exist between $\psi(3684)$ and $\psi(3095)$.

(2) The question of the other decay modes of the $\psi(3684)$ is somewhat puzzling. Figure 30 illustrates this in connection with four-prong events of zero total charge, and makes a comparison between $\psi(3095)$ and $\psi(3684)$ decay modes. In particular Fig. 30a [$\psi(3095)$ decay] and Fig. 30d [$\psi(3684)$ non-cascade decay] show strong differences, such as the suppression in the case of the $\psi(3684)$ of the $2\pi^+2\pi^-\pi^0$ decay mode which is very prominent in the $\psi(3095)$ as the slanted band of points on the right side of Fig. 30a. Thus although one might have naively expected that the partial widths for various hadronic modes ought, because of increased phase space, to be at least as large in $\psi(3684)$ as in $\psi(3095)$, this does not appear to be true. The branching ratio measurements for various exclusive $\psi(3684)$ decay modes are presently in progress, but it appears that the branching ratios for modes which are prominent in $\psi(3095)$ decay are very small here.

E. Summary

We can briefly summarize the main conclusions from data discussed in this lecture:

- (1) From both the photoproduction data and the study of the hadronic decay modes, the ψ particles appear to be hadrons.
- (2) Both ψ particles have $I = 0$, $G = -1$.
- (3) There is no indication that single photon emission is the dominating feature of $\psi(3095)$ decay.
- (4) The cascade decay, $\psi(3684) \rightarrow \pi\pi\psi(3095)$, is less inhibited than other hadron decay modes of either ψ particles.

(5) The non-cascade $\psi(3684)$ decay modes do not look like the dominant $\psi(3095)$ modes.

III. ARE THERE OTHER STATES IN THE NEW SPECTROSCOPY?

A. Search for Narrow Resonances Coupled to e^+e^-

Only two narrow massive resonances have been established so far, the $\psi(3095)$ and $\psi(3684)$. However the "fine-energy scan" operation mode already described in the first lecture has been used to search for other such states both at SPEAR and at ADONE.^{30,36} Such a scan can be used to set an upper limit to [see Eq. (4)]

$$I \equiv \int \sigma_{\text{hadrons}}^R dW = \frac{2\pi^2}{M^2} (2J+1) \frac{\Gamma_e \Gamma_{\text{hadrons}}}{\Gamma}$$

If one assumes $J = 1$, $\Gamma_{\text{hadrons}}/\Gamma \approx 1$,

$$\Gamma_e = \frac{M^2}{6\pi^2} I \quad (33)$$

and therefore the scan sets an upper limit to Γ_e for any narrow resonance. It is important to note that this technique which depends on the observation of a large resonant cross section at one or two neighboring energies of the scan does not detect broad resonances. The resulting upper limits given in Table VIII cover, with the exception of a couple of holes, the energy region between 1.91 and 7.6 GeV. There seem to be no additional states with values of Γ_e comparable to those of the already identified resonances.

B. Search for Wide Resonances Coupled to e^+e^-

The results of measurements of σ_{hadrons} by e^+e^- annihilation are shown^{21,38} in Fig. 31. Most of the data come from a not-so-fine scan with fairly substantial statistics from 2.6 to 7.4 GeV by the SLAC-LBL group. There is a clear structure at $M = 4100$ MeV which, if interpreted as a resonance, has a width $\Gamma \approx 250$ MeV. Assuming a spin $J = 1$, the value of Γ_e as determined from (33) is about 4 keV, which is comparable to the value for the narrow ψ resonances as well as for the ρ , ω and ϕ . This structure is presently under extensive study, and nothing more can be said about it now except to note that it falls a bit higher than the $\psi(3684)$ and would fit extremely well into a picture in which a new

threshold were opening up between 3.7 and 4 GeV. If this threshold represents the masses of pairs of particles into which the ψ 's like to decay, one might be able to interpret why the lowest two states are very narrow and the state at 4100 MeV is quite broad. Such a picture would also explain in a natural way the increase in the ratio

$$R \equiv \frac{\sigma_{\text{hadrons}}}{\sigma_{\mu\mu}} \quad (34)$$

seen in Fig. 31b from its value of about 2 below $W = 3.5$ GeV to its value of about 5 above $W = 4.5$ GeV. This question of the energy dependence of R is evidently closely related to the new spectroscopy, but we have no time here to dwell on it in any detail.

C. The Charmed Quark

To proceed further in discussing the evidence for new states, it is most convenient to introduce that model which has so far provided the most natural interpretation for the narrow width of the ψ 's. I shall do so here only to the extent and with the degree of detail necessary to interpret the experimental results leaving to Professor Harari the task of filling in further details.

When Table I was introduced in the first lecture, we discussed only the u , d , s quarks listed in the first three lines, which account for the states of the "old spectroscopy." It is now desirable to introduce the fourth quark c which is an $SU(3)$ singlet carrying a new additive quantum number, Charm, which, like strangeness, is assumed to be conserved in all but the weak interactions. One of the original motivations for introducing the charmed quark, long before the discovery of ψ 's, was the nice symmetry it provided between the four known leptons and four quarks.³⁹ Furthermore, as will be seen a little further, with an appropriate form of the weak interaction current, one could account for the large suppression of strangeness changing weak neutral currents relative to strangeness conserving weak neutral currents.⁴⁰

With the charmed quark, the baryon and meson states are still represented by qqq and $q\bar{q}$ combinations, but the Gell-Mann/Nishijima formula becomes:

$$Q = I_3 + Y/2 + \frac{2}{3} C, \quad (35)$$

where C is the charm. Note that charmed particles (i.e., $C \neq 0$) have fractional hypercharge.

It is interesting to consider what new states are made possible by the introduction of the charmed quark. This is discussed in detail in the review paper of Gaillard, Lee and Rosner⁴¹ and we confine ourselves here to showing in Table IX the additional meson states which contain at least one charmed quark. Since the ψ 's couple to photons, they cannot be particles with nonzero charm, but they can be interpreted as ϕ_c , vector bound states of $c\bar{c}$. In this picture, the very small width can be interpreted in terms of Zweig's rule,⁴ as already described for the ordinary ϕ , forbidding decays into the usual hadrons, the allowed decay modes being those into pairs of charmed mesons (in the same sense that the allowed ϕ decay is into a pair of K mesons). If the lightest charmed mesons have masses which are greater than $\frac{3684}{2} = 1842$ MeV, these allowed decay modes are kinematically inaccessible and the long ψ lifetimes are at least qualitatively interpreted. In this picture then, the $\psi(3095)$ represents a bound $c\bar{c}$ state with the same quantum numbers and in the same sense that the ϕ represents an $s\bar{s}$ state. The large ψ mass is interpreted in terms of a mass for the charmed quark which is much larger than the masses of the u, d, s quarks. If we consider quadratic mass formulas and take account of the fact that the D or F charmed mesons of Table IX would contain one c quark whereas the ψ has two of them, a very simple estimate of the mass of a charmed meson would be obtained as follows,

$$m_{D,F}^2 - m_\rho^2 \approx \frac{1}{2} (m_\psi^2 - m_\rho^2), \quad (36)$$

hence $m_{D,F}^2 \approx 0.6 + \frac{1}{2}(9.6 - 0.6) \approx 5 \text{ GeV}^2$, $m_{D,F} \approx 2.3 \text{ GeV}$.

This figure satisfies the condition of being greater than 1842 MeV, and is in fact also a little too large to satisfy the condition for a threshold at about 4.0 GeV suggested by the data of Fig. 31. However, given the gross uncertainties of the estimate (36), there is no problem here.

D. $c\bar{c}$ Spectroscopy

In direct analogy with the usual quark model, one can construct low-lying meson states arising from bound $c\bar{c}$ quarks. These are shown in Table X. The 1^{--} state is of course the $\psi(3095)$. The $\psi(3684)$ is assumed to be a radial excitation, with the same $L = 0$, $S = 1$ as the $\psi(3095)$, on the grounds that the value of Γ_e is large enough to suggest a wave function which is nonvanishing at the origin. Although there is not enough knowledge to permit sure prediction of the masses of these states, it seems reasonable to suppose that they mostly lie below the $\psi(3684)$ (by analogy with the fact that corresponding states with u , d , s quarks lie below the ρ' , the radial excitation of the ρ), and hence that they are states of very narrow width.

Since the states other than the ψ do not have the photon quantum numbers, it is not surprising that they are not directly formed in e^+e^- annihilation and hence not found in the scans summarized in Table VIII. Other ways of searching for them is through their production in strong interaction experiments, or via decays of ψ 's formed in annihilation. The problem in the strong interaction experiments arises from the fact that it is difficult to set up experiments to search for decay modes more complex than two-body modes such as $p\bar{p}$, and that the product of cross section times branching ratio for such simple modes is likely to be so small as to be inseparable from the general two-body hadronic background. In any case we postpone discussion of searches for narrow states produced by hadronic processes until Sec. E2.

A perhaps more promising avenue for finding other $c\bar{c}$ bound states is to look for them among decay products of the ψ particles. The combination

of isospin and G parity selection rules with the smallish (\sim a few hundred MeV) mass differences expected do not allow much in the way of hadronic decay modes, but electromagnetic decays with the emission of a monochromatic photon are in principle possible for all even charge conjugation states in Table X. Since the overall widths of the ψ 's are small, the branching ratios for such electromagnetic decays might well be sizable.⁴² The most natural supposition is that most of the states, particularly those with $L = 1$ lie above the $\psi(3095)$ and hence are best searched for in the decays of the $\psi(3684)$.

At the time that these lectures were delivered, the only generally available result of such a search was that of the HEPL Group at SPEAR⁴³ which detected and measured the energies of photons emitted in $\psi(3684)$ decay by means of two NaI crystal spectrometers located on the two sides of the East Interaction Region. Results for photon energy spectra are shown in Fig. 32. The "unconverted" spectra are those of highest resolution (4.5% FWHM), the "converted" spectra corresponding to resolutions varying from 13.5% FWHM at 100 MeV to 6% FWHM above 400 MeV. The spectra of Fig. 32 are not truly inclusive because of trigger requirements and are convertible into upper limits for monochromatic photon production only in a somewhat model-dependent way. Although the HEPL group placed specific limits for specific photon energy ranges, it is probably adequate here to summarize their result as roughly 99% C.L. upper limits of 5 - 10% for the branching of $\psi(3684)$ into any particular decay which produces a monoenergetic photon between 600 and 75 MeV, the best limits corresponding to the highest photon energies. Obviously the sensitivity for a given resolution is limited by the π^0 background which accounts for the spectra in Fig. 32.

One way of decreasing the π^0 background is to search for more specific sorts of decay modes for the states of interest in association with monochromatic gamma rays. A specific case in point has already been discussed, namely the cascade decay mode [see Eq. (32)],

$$\begin{aligned}
 \psi(3684) &\rightarrow \chi + \gamma_1 \\
 &\quad | \rightarrow \psi(3095) + \gamma_2 \\
 &\quad \quad | \rightarrow \mu^+ \mu^- \text{ or } e^+ e^-
 \end{aligned}
 \tag{32}$$

The DESY-DASP group⁴⁴ has reported evidence for such a radiative cascade with the photon energies at 160 and 420 MeV indicating for the intermediate a mass of either 3.52 or 3.26 GeV [depending on which photon energy corresponds to γ_1 and which corresponds to γ_2 in (32)]. Further details are given in H. Oberlack's talk at the Topical Conference. It is however interesting to note that this process is consistent with the roughly uniform part of the shaded population shown in Fig. 29. The branching ratio for the decay mode (32) as estimated by the DASP group or from the data of Fig. 29 amounts to a few percent. Coupled with the above inclusive photon limits, it leads to the conclusion that the radiative decay to $\psi(3095)$ is a major or dominant decay mode of the particular intermediate state observed.

Other possible decay modes of the intermediate states might be

$$\chi \rightarrow \pi^+ \pi^-, K^+ K^-, 2\pi^+ 2\pi^-, 3\pi^+ 3\pi^-, \pi^+ \pi^- K^+ K^-, \text{ etc.}$$

Evidence for states at 3.41 and 3.53 GeV decaying via some of these modes has, after the end of these lectures, been reported by the SLAC-LBL group.⁴⁵ Confirmation of the radiative cascade modes has also been provided.⁴⁶ The interested reader is referred to the published papers and the Stanford Symposium on Lepton and Photon Interactions for details. Here I just want to make one further point. Although the discovery of such states is consistent with the charmed quark hypothesis it does not establish it in any sense. There is after all, on almost any model of the ψ particles as hadrons, no reason to suppose that the spectroscopy is limited to $J^{PC} = 1^{--}$ states. The real test of the charm hypothesis must come from the actual discovery of charmed particles decaying via the weak interaction. It is to the search for such particles that we now turn our attention.

E. Charmed Particles

1. Decay Properties of Charmed Particles

The form of the weak interaction with the inclusion of charmed quarks is a subject of continuing theoretical interest. We consider here the form of the current proposed by Glashow et al.,⁴⁰

$$J = \bar{c}O[-d \sin \theta_c + s \cos \theta_c] + \bar{u}O[d \cos \theta_c + s \sin \theta_c] \quad (37)$$

where $O \equiv \gamma_\mu(1 + \gamma_5)$ and $\theta_c =$ Cabbibo angle. As pointed out by Glashow et al. this current has the valuable property of cancelling out contributions from the strangeness-changing weak neutral currents while permitting the existence of strangeness-conserving weak neutral currents. The smallness of the Cabbibo angle θ_c permits a useful hierarchy of decay amplitude strengths which are summarized in Table XI. Estimates of actual amplitudes and rates require more detailed considerations than provided by Table XI but general qualitative features can be obtained from the Table. In particular, the leading amplitudes ($\cos \theta_c$ or $\cos^2 \theta_c$) in charm-changing decays are those for which $\Delta S = \Delta C$. Thus from nonstrange charmed mesons, one would expect decays which favor production of a strange particle. Some typical preferred charmed meson decay modes and roughly estimated decay rates from Gaillard et al.⁴¹ are given in Table XII.

2. Search for States of Sharply Defined Mass Which are Decay

Products of Charmed Particles

Since charmed particles are long lived, they have sharply defined masses. One can search for them by measuring effective masses of various particle combinations detected in an appropriate apparatus. We consider such searches in both hadron-initiated and e^+e^- initiated final states.

(a) Hadron Initiated Final States

Typical experiments consist of magnetic spectrometers of good resolution looking at final states of the form:

$$\text{hadron} + \text{nucleus} \rightarrow A^+ + B^- + \text{anything}$$

where A, B are π^\pm , K^\pm , p, \bar{p} and may be the products of decays of the form

$$D \rightarrow A^+ + B^- .$$

The difficulty in obtaining high sensitivity in such experiments is the very large background of hadron pairs A^+B^- of practically all kinematically allowed masses. For example, Winkelmann et al.⁴⁷ have found that for

$$\pi^- + p \rightarrow \pi^+ + \pi^- + \text{anything}$$

with 205 GeV incident pions, the total inclusive cross section for making $\pi^+\pi^-$ pairs of invariant mass near 2.5 GeV is roughly

$$\frac{d\sigma}{dM} \approx 15 \mu\text{b/MeV} ,$$

which is of course a very large background, even for a spectrometer of high resolution. It is possible to greatly improve the sensitivity by searching for diparticle states which decay at about 90° relative to the beam direction. Such states will have decay products of high transverse momentum, and the continuous hadron background will be reduced by several orders of magnitude. In this way it is possible to arrive at sensitivities for the detection of charmed particles of less than one microbarn. There is further sensitivity improvement if Cerenkov counters are used for particle identification. We now discuss two specific experiments.

The MIT-BNL group has searched for narrow states in the mass range 1.2-5 GeV from combinations of π^+ , K^+ , p with π^- , K^- , \bar{p} produced by interactions of 30 GeV protons on beryllium. Typical results are shown in Figs. 33 and 34 for $\bar{p}p$ and $K^+\pi^-$ respectively.^{6,48} No significant signal has been detected, at least between 2 and 3.5 GeV where the analysis has been completed, and the sensitivities vary from about 0.04 nb (π^+K^- , $\pi^+\bar{p}$ at 3.1 GeV) to 40 nb ($p\pi^-$ at 2.25 GeV). This search can also serve to find not only charmed states, but also ψ -like states with quantum numbers different from the photon. The obvious difficulty of the search is well illustrated by the $\bar{p}p$ data; it is in fact known that the $\psi(3095)$ is produced and decays into $\bar{p}p$ with a branching ratio of 0.2%; yet no signal

is seen because the sensitivity (0.4 nb) is insufficient by about two orders of magnitude. The lesson is that two-body branching ratios are probably small and unless cross sections are large, it is difficult to have an adequate sensitivity.

At higher energy, the FNAL-Northwestern-Rochester-SLAC group⁴⁹ have looked for similar two-body final states produced by collisions of 200 GeV neutrons on beryllium. Looking for diffractive-like low multiplicity events (without benefit of Cerenkov counters unlike the MIT-BNL group) they set typical upper limits of 150-50 nb for masses in the 2-3.5 GeV range.

There have been some searches into multiparticle final states, but with much less sensitivity. For example, Baltay et al.⁵⁰ report limits from 15 GeV incident π^+ in a hydrogen bubble chamber of the order of a few μb for each channel studied.

(b) e^+e^- Initiated Final States

As was noted in connection with the data of Fig. 31, the measured ratio $R \equiv \sigma_{\text{hadrons}}/\sigma_{\mu\mu}$ undergoes just above the mass of the $\psi(3684)$ a rapid and substantial rise followed by the broad 4100 MeV structure. Furthermore there appear to be no narrow states of higher mass. The natural interpretation of this effect is the crossing of threshold for production of charmed meson pairs around 4 GeV. Furthermore if one associates the change in R, $\Delta R \approx 2$ with the production of charmed particle pairs, one has an effective cross-section prediction for these pairs of about $2\sigma_{\mu\mu}$. At $W = 4.8$ GeV, where substantial data have been accumulated, this cross section corresponds to roughly 7 nb out of a total cross section to hadrons of about 20 nb.

The SLAC-LBL group has searched for narrow effective mass peaks in $K^{\pm}\bar{\pi}$, $K_S^0\pi^+\pi^-$, $\pi^+\pi^-$, $K^+\bar{K}^-$, $K^{\mp}\pi^{\pm}\pi^{\pm}$, $K_S^0\pi^{\pm}$, $\pi^+\pi^-\pi^{\pm}$ states.⁵¹ No Cerenkov or time-of-flight particle identification was available and K_S^0 were identified, with significant background, by cuts on $\pi^+\pi^-$ effective mass. Typical

mass resolutions for the above combinations were 80 MeV FWHM for two-particle and somewhat better for three-particle final states. The data are shown in Fig. 35. Typical results at the 90% confidence level, are as follows:

$$\frac{1}{2}\sigma(K^{\mp}\pi^{\pm}, \bar{K}^0\pi^+\pi^-, K^0\pi^+\pi^-) < 0.45 \text{ nb}$$

$$\frac{1}{2}\sigma(K^+K^-, \pi^+\pi^-) < 0.08 \text{ nb}$$

$$\frac{1}{2}\sigma(K^{\pm}\pi^{\pm}\pi^{\pm}, \bar{K}^0\pi^{\pm}, K^0\pi^{\pm}) < 0.26 \text{ nb}$$

$$\frac{1}{2}\sigma(\bar{K}^0K^{\pm}, K^0K^{\pm}, \pi^+\pi^-\pi^{\pm}) < 0.38 \text{ nb} ,$$

all in the mass range 1.85 - 2.40 GeV. The factor 1/2 is put in because the charmed particles are assumed to be produced in pairs. Thus typical branching ratios of the D mesons into preferred modes like $K\pi$ and $K\pi\pi$ appear small ($\lesssim 10\%$). Higher multiplicity, all-charged particle final states have also been searched for with no signal seen. It is interesting to note the absence of significant inclusive $\psi(3095)$ production, which would be seen via its $\mu^+\mu^-$ decay mode as a spike near 3.1 GeV in the $\pi^+\pi^-$ data.

The nice feature of searching for charmed particles in the annihilation data is that there is a basis for predicting the cross section. Branching ratios can only be estimated in a model dependent way; but any future substantial improvements in the above upper limits may pose serious difficulties for charm models.

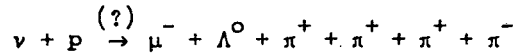
3. Search for Evidence of Charmed Particle Production in Neutrino Processes

(i) Manifestation via Apparent Violation of $\Delta S = \Delta Q$ Rule

Consider neutrinos incident on liquid hydrogen producing the reaction, $\nu p \rightarrow \mu^- B_c^{++}$ where B_c^{++} is a charmed baryon. According to Table XI a baryon with $S = 0$, $C = +1$ can be produced via a $\sin \theta_c$ amplitude. (Note that $|\Delta \vec{I}| = 1/2$ is satisfied because B_c^{++} is the $I_3 = 1$ member of an isovector state formed by the quark combination $(cuu)^{++}$.) Referring again to Table XI, B_c^{++} can decay to normal hadrons via a $\Delta S = \Delta C = -1$ transition with

a $\cos^2 \theta_c$ amplitude, leaving a final hadron state of charge +2 and strangeness -1, hence a state which violates the $\Delta S = \Delta Q$ rule of usual weak interactions.

A rather remarkable candidate for this sort of process has been reported from a BNL experiment with the 7-foot bubble chamber⁵²:



the mass of the final hadron state being 2426 ± 12 MeV. Crucial to this interpretation is the absence of a K meson either as an undetected neutral, or as one of the observed positive particles. Unfortunately no really convincing case can be made from a single event of this sort.

In a νp experiment in the FNAL 15-foot chamber with higher energy neutrinos,⁵³ two events with a Λ decay and no undetected neutrals have been observed; in both cases one of the accompanying positive particles was required by the kinematics to be a K meson. As more data accumulate, it will be interesting to see if any more events of the type observed at BNL turn up.

(ii) Dimuon Production

Going back to our process $\nu p \rightarrow \mu^- B_c^{++}$, the charmed baryon can undergo semileptonic decay, $B_c^{++} \rightarrow \mu^+ + B^+ + \nu$, where as required by Table XI, $\Delta C = \Delta Q = -1$. This mechanism produces dimuons of opposite charge only with a cross section proportional to $\sin^2 \theta_c$. Thus roughly 5% of the charged current neutrino events of high energy might produce charmed particles, of which perhaps 10% would lead to semileptonic decays and hence muon pairs. One might thus expect a muon pair rate of the order of 0.5%. The experimental difficulty in the observation of such events is of course to establish that the additional muons do not arise from decays of pions or kaons in the outgoing hadron jet.

Benvenuti et al.⁵⁴ have reported the observation of 14 events with $\mu^+ \mu^-$ pairs from ν and $\bar{\nu}$ incident beams. The absence of dimuons of the same charge, plus studies of p_{\perp} distributions lead this group to conclude

that most of their events do not come from pion or kaon decay. Furthermore the absence of trimuons suggest a missing ν or $\bar{\nu}$ as predicted above. The rate is about 0.9% of charged current neutrino events above 40 GeV, which is roughly consistent with expectations from the charm picture as discussed above. There are alternative interpretations such as the production of heavy leptons decaying via $\mu^+ \mu^- \nu$, but the charm explanation seems to be preferred. Although indirect, these data may provide some of the best evidence for the existence of charmed particles. Hopefully neutrino bubble chamber experiments with neon-hydrogen fills aimed at searching for μ -e (because electrons are easier to recognize in a neon-filled bubble chamber than muons) pairs may help firm up the interpretation of the dimuon events.

4. Other Methods of Searching for Charmed States

Other approaches have been or are being pursued to search for charmed states or other new types of particles. These include:

(i) Search for enhanced production of strange particles coupled to other symptoms of possible charm such as the presence of a lepton in a hadron-produced initiated process or being just above the apparent threshold energy $W \approx 4$ GeV in e^+e^- annihilation.

(ii) Attempts at studying and understanding direct lepton production in hadron processes. Such production appears to be in excess of the expectations from ρ , ω , ϕ and ψ production.⁵⁵

(iii) Study of the production of μ^+e^- (plus undetected neutrals) in e^+e^- annihilation. A report on this work will be made by Martin Perl in the Topical Conference.

(iv) Search for decays of lifetime $\sim 10^{-13}$ sec corresponding to flight paths of about 30 microns in photographic emulsion. The problem here is to establish that such events are not neutron stars or decays of Λ , K_S^0 or K_L^0 . This can be done if there are enough events, or if pairs of short-lived particles are observed. Several experiments of this sort are planned at Fermilab.

As of this time, none of these approaches has yet given a conclusive charmed particle signal.

ACKNOWLEDGMENT

I want to express my particular indebtedness to my colleagues in the SLAC-LBL collaboration not only for supplying an important fraction of the physics discussed in these lectures, but for explaining to me many of the interpretive features presented here. The membership of that collaboration includes or has included the following physicists: G. S. Abrams, J.-E. Augustin, A. M. Boyarski, M. Breidenbach, D. D. Briggs, F. Bulos, W. Chinowsky, J. T. Dakin, G. J. Feldman, G. E. Fischer, C. E. Friedberg, D. Fryberger, G. Goldhaber, G. Hanson, R. J. Hollebeek, B. Jean-Marie, A. D. Johnson, J. A. Kadyk, R. R. Larsen, A. M. Litke, D. Lüke, B. A. Lulu, V. Lüth, H. L. Lynch, D. Lyon, C. C. Morehouse, J. M. Paterson, M. L. Perl, F. M. Pierre, T. Pun, P. Rapidis, B. Richter, B. Sadoulet, R. F. Schwitters, W. M. Tanenbaum, F. Vannucci, J. S. Whitaker, F. C. Winkelmann, J. E. Wiss, and J. E. Zipse.

I also want to express my special thanks to Miss Christina Frank for her exceptional work and patience in getting this manuscript together.

FOOTNOTES AND REFERENCES

1. The charmed quark c in the fourth row of Table I will be discussed later.
2. F. J. Gilman, SLAC-PUB-1532 (January 1975).
3. There is a regrettable notational confusion between the charge conjugation quantum number C and the charm quantum number C . I have not attempted to use a different symbol for either of these quantities, but hope that from their usage the meaning will be self-evident.
4. G. Zweig, CERN Preprints TH 401 and TH 412 (1964), unpublished. For a recent discussion, see F. Gilman, SLAC-PUB-1537 (1975).
5. J. J. Aubert et al., Phys. Rev. Letters 33, 1404 (1974).
6. S. C. C. Ting, Rapporteur's Summary at the International Conference on High Energy Physics, Palermo, Sicily, June 1975.
7. J. J. Aubert et al., Nuclear Physics B89, 1 (1975).
8. J.-E. Augustin et al., Phys. Rev. Letters 33, 1406 (1974).
9. C. Bacci et al., Phys. Rev. Letters 33, 1408 (1974).
10. G. S. Abrams et al., Phys. Rev. Letters 33, 1453 (1974).
11. L. Criegee et al., Physics Letters 53B, 489 (1975).
12. B. Knapp et al., Phys. Rev. Letters 34, 1040 (1975).
13. W. Braunschweig et al., Physics Letters 56B, 491 (1975).
14. J.-E. Augustin et al., Phys. Rev. Letters 34, 233 (1975).
15. W. Braunschweig et al., Physics Letters 53B, 491 (1975).
16. R. L. Ford et al., Phys. Rev. Letters 34, 604 (1975).
17. Y. S. Tsai, J. D. Jackson, SLAC-PUB-1515 (1974); D. R. Yennie, Phys. Rev. Letters 34, 239 (1975).
18. A. M. Boyarski et al., Phys. Rev. Letters 34, 1357 (1975).
19. V. Lüth et al., SLAC-PUB-1617 and LBL-4211 (1974), to be published in Phys. Rev. Letters.
20. C. Bacci et al., Frascati Preprint LNF-75/35(P) (1975).
21. J.-E. Augustin et al., Phys. Rev. Letters 34, 764 (1975).

22. M. Jacob and G. C. Wick, *Annals of Physics* 7, 404 (1959).
23. K. Gottfried and J. D. Jackson, *Nuovo Cimento* 33, 309 (1964).
24. B. Knapp et al., *Phys. Rev. Letters* 34, 1044 (1975).
25. F. W. Büsser et al., *Physics Letters* 56B, 482 (1975).
26. G. J. Blunar et al., *Phys. Rev. Letters* 35, 346 (1975).
27. See for example S. C. C. Ting, *Proceedings of the 14th International Conference on High Energy Physics* (1968).
28. B. Gittelman et al., *Contribution to Palermo Conference* (1975).
29. U. Camerini et al., *Phys. Rev. Letters* 35, 483 (1975).
30. A. M. Boyarski et al., SLAC-PUB-1599, LBL-3897, *Contribution to Palermo Conference* (1975).
31. W. Braunschweig et al., *Physics Letters* 57B, 297 (1975).
32. G. Goldhaber et al., *Proceedings of the IVth International Nucleon-Antinucleon Symposium, Syracuse, NY, LBL-4224, SLAC-PUB-1622* (1975).
33. F. Gilman, private communication.
34. G. S. Abrams et al., *Phys. Rev. Letters* 34, 1181 (1975).
35. J. A. Kadyk et al., *Proc. Xth Rencontre de Moriond, LBL-3687* (1975).
36. A. M. Boyarski et al., *Phys. Rev. Letters* 34, 762 (1975).
37. C. Bacci et al., submitted to *Physics Letters* (1975).
38. G. J. Feldman, SLAC-PUB-1624, *Contribution to Palermo Conference* (1975).
39. J. D. Bjorken and S. L. Glashow, *Phys. Rev. Letters* 11, 255 (1964).
40. S. L. Glashow, J. Iliopoulos and L. Maiani, *Phys. Rev.* D2, 1285 (1970).
41. M. K. Gaillard, B. W. Lee and J. L. Rosner, *Rev. Mod. Physics* 47, 277 (1975).
42. T. Appelquist et al., *Phys. Rev. Letters* 34, 365 (1974); E. Eichten et al., *Phys. Rev. Letters* 34, 369 (1974).
43. J. W. Simpson et al., *Phys. Rev. Letters* 35, 699 (1975).
44. W. Braunschweig et al., *Physics Letters* 57B, 407 (1975).
45. G. Feldman et al., *Phys. Rev. Letters* 35, 821 (1975).

46. W. Tanenbaum et al., SLAC-PUB-1644, LBL-4253 (1975).
47. F. Winkelmann et al., Physics Letters 56B, 101 (1975).
48. J. J. Aubert et al., Phys. Rev. Letters 35, 416 (1975).
49. E. J. Bleser et al., Phys. Rev. Letters 35, 76 (1975).
50. C. Baltay et al., Phys. Rev. Letters 34, 1118 (1975).
51. A. M. Boyarski et al., Phys. Rev. Letters 35, 195 (1975).
52. E. G. Cazzoli et al., Phys. Rev. Letters 34, 1125 (1975).
53. Private communication from E-45 Group.
54. A. Benvenuti et al., Phys. Rev. Letters 34, 419 (1975).
55. See L. Lederman's Paper at the Stanford Symposium on Lepton and Photon Interactions (1975).

Table I. Quark properties.

Quark	Spin	I	I_3	Q	S	B	Y	Charm
u	1/2	1/2	1/2	2/3	0	1/3	1/3	0
d	1/2	1/2	-1/2	-1/3	0	1/3	1/3	0
s	1/2	0	0	-1/3	-1	1/3	-2/3	0
c	1/2	0	0	2/3	0	1/3	0	1

Table II. $L = 0$ meson states.

SU(6) multiplet	SU(3) multiplet	Spin	J^{PC}	States
1	1	0	0^{-+}	η'
35	8	0	0^{-+}	π, η, K
	$8 + 1$	1	1^{--}	ρ, ω, ϕ, K^*

Table III. $\psi(3095)$ properties.

	SLAC-LBL	Frascati
Mass	3.095 ± 0.004 GeV	3.103 ± 0.008 GeV
J^{PC}	1^{--}	
Γ	69 ± 15 keV	68 ± 26 keV
Γ_e	4.8 ± 0.6 keV	4.6 ± 0.8 keV
Γ_μ	4.8 ± 0.6 keV	Assumed equal to Γ_e
$\Gamma_{\gamma h}$	12 ± 2 keV	
Γ_e/Γ	0.069 ± 0.009	
Γ_μ/Γ	0.069 ± 0.009	

Table IV. $\psi(3684)$ properties.

Mass	3.684 ± 0.005 GeV
J^{PC}	1^{--}
Γ	228 ± 56 keV
$\Gamma_e = \Gamma_\mu$	2.1 ± 0.3 keV
$\Gamma_{\gamma h}$	7 ± 1.2 keV
$\frac{\Gamma_e}{\Gamma} = \frac{\Gamma_\mu}{\Gamma}$	0.0093 ± 0.0016

Table V. Decay modes of the $\psi(3095)$.

Mode	Branching ratio (%)	No. of events observed	Comments
e^+e^-	6.9 ± 0.9	ca. 2000	
$\mu^+\mu^-$	6.9 ± 0.9	ca. 2000	
$\pi^+\pi^-$	$< 0.032^*$		90% C.L.
$\rho\pi$	1.3 ± 0.3	153 ± 13	$> 70\%$ of $\pi^+\pi^-\pi^0$
$2\pi^+2\pi^-$	0.4 ± 0.1	76 ± 9	
$2\pi^+2\pi^-\pi^0$	4.0 ± 1.0	675 ± 40	{ 20% $\omega\pi^+\pi^-$ 30% $\rho\pi\pi$
$3\pi^+3\pi^-$	0.4 ± 0.2	32 ± 7	
$3\pi^+3\pi^-\pi^0$	2.9 ± 0.7	181 ± 26	
$4\pi^+4\pi^-\pi^0$	0.9 ± 0.3	13 ± 4	
$\pi^+\pi^-\bar{K}^+K^-$	0.4 ± 0.2	83 ± 18	{ not including $K^*(892)K^*(1420)$
$2\pi^+2\pi^-\bar{K}^+K^-$	0.3 ± 0.1		
K^+K^-	$< 0.058^*$		90% C.L.
$K_S^0K_L^0$	< 0.02	≤ 1	90% C.L.
$K^0K^{0*}(892)$	0.24 ± 0.05	57 ± 12	
$K^\pm K^{\mp*}(892)$	0.31 ± 0.07	87 ± 19	
$K^0K^{0*}(1420)$	< 0.19	≤ 3	90% C.L.
$K^\pm K^{\mp*}(1420)$	< 0.19	≤ 3	90% C.L.
$K^{*0}(892)\bar{K}^{*0}(892)$	< 0.06	≤ 3	90% C.L.
$K^{*0}(1420)\bar{K}^{*0}(1420)$	< 0.18	≤ 3	90% C.L.
$K^{*0}(892)K^{*0}(1420)$	0.37 ± 0.10	30 ± 7	
$p\bar{p}$	0.21 ± 0.04	105 ± 11	{ assuming $f(\theta) \sim 1 + \cos^2\theta$
	$0.25 \pm 0.07^*$		
$\Lambda\bar{\Lambda}$	0.16 ± 0.08	19 ± 5	
$p\bar{p}\pi^0$	0.37 ± 0.19	87 ± 30	
$n\bar{n}\pi^-$			
$\bar{p}n\pi^+$			

*Results from DESY-DASP.³¹ Others are from SLAC-LBL.³⁰

Table VI. SU(3) singlet tests for $\psi(3095)$.

Decay mode	Relative SU(3) singlet prediction	Observed branching ratio ^a
Forbidden modes:		
$\pi^+ \pi^-$	0	< 0.032%
$K^+ K^-$	0	< 0.08%
$K_L^0 K_S^0$	0	< 0.02%
$K^0(892) \bar{K}^0(892)$	0	< 0.06%
$K^0(1420) \bar{K}^0(1420)$	0	< 0.18%
$K^+ K^- (1420)$	0	< 0.19%
$K^0 K^0(1420)$	0	< 0.19%
Non-forbidden modes for comparison:		
$K^0 K^0(892)$	1	$0.24 \pm 0.05\%$
$K^+ K^- (892)$	1	$0.31 \pm 0.07\%$
$K^0(892) K^0(1420)$	no prediction	$0.37 \pm 0.10\%$
$\rho \pi$	3/2	$1.3 \pm 0.3\%$

^aThe $\pi^+ \pi^-$ and $K^+ K^-$ branching ratios are from DESY-DASP.³¹ The others are from SLAC-LBL.³⁰

Table VII. Branching ratios for $\psi(3684)$ decay.

Modes	Branching ratio (%)	Comments
e^+e^- or $\mu^+\mu^-$	0.93 ± 0.16	
$\psi(3095) + \text{anything}$	57 ± 8	
$\psi(3095)\pi^+\pi^-$	32 ± 4	These decays included in fraction for $\psi(3095) + \text{anything}$
$\psi(3095)\eta$	4 ± 2	
$\rho^0\pi^0$	< 0.1	90% C.L. based on preliminary analysis
$2\pi^+2\pi^-\pi^0$	< 0.7	
$p\bar{p}$	< 0.03	
$\pi^+\pi^-$	$< 0.09^*$	
K^+K^-	$< 0.16^*$	

*The $\pi^+\pi^-$ and K^+K^- limits are from the DESY-DASP experiment. The other branching ratios are from the SLAC-LBL data. Several of these have been independently determined by the DESY-DASP collaboration, and are in good agreement with the above values.

Table VIII. Fine scan results.

Storage ring	Mass range (GeV)	Upper limits	
		I (nb-MeV)	Γ_e (keV)
ADONE	1.910 - 2.20	950	0.17
	2.20 - 2.545	660	0.16
	2.97 - 3.09	830	0.33
SPEAR	3.2 - 3.5	970	0.47
	3.5 - 3.68	780	0.44
	3.72 - 4.0	850	0.55
	4.0 - 4.4	620	0.47
	4.4 - 4.9	580	0.54
	4.9 - 5.4	780	0.90
	5.4 - 5.9	800	1.11
5.9 - 7.6	450	0.87	

Table IX. Meson states with ≥ 1 charmed quark.

Quark content	Name		I	Charm	Strangeness
	Pseudoscalar	Vector			
$(c\bar{d})^+, (c\bar{u})^0$	D^+, D^0	D^{*+}, D^{*0}	1/2	+1	0
$(\bar{c}u)^0, (\bar{c}d)^-$	\bar{D}^0, D^-	\bar{D}^{*0}, D^{*-}	1/2	-1	0
$(c\bar{s})^+$	F^+	F^{*+}	0	+1	+1
$(\bar{c}s)^-$	F^-	F^{*-}	0	-1	-1
$(c\bar{c})^0$	η_c	ϕ_c	0	0	0

Table X. Lowest lying $c\bar{c}$ states.

L	S	J^{PC}	G	I
0	0	0^{-+}	+1	0
0	1	1^{--}	-1	0
1	0	1^{+-}	-1	0
1	1	0^{++}	+1	0
1	1	1^{++}	+1	0
1	1	2^{++}	+1	0

Table XI. Charmed particle decay selection rules.

Amplitude dependence on θ_C	Selection rules
<u>Leptonic or semileptonic decays</u>	
$\cos \theta_C$	$\Delta S = \Delta C = \Delta Q = \pm 1, \Delta I = 0$ or $\Delta S = \Delta C = 0, \Delta Q = \pm 1, \Delta I = 1$
$\sin \theta_C$	$\Delta S = 0, \Delta C = \Delta Q = \pm 1$ or $\Delta S = \Delta Q = \pm 1, \Delta C = 0$ $ \Delta I = \frac{1}{2}$
<u>Hadronic decays</u>	
$\cos^2 \theta_C$	$\Delta S = \Delta C = \pm 1, \Delta I = 1$
$\cos \theta_C \sin \theta_C$	$\Delta S = 0, \Delta C = \pm 1, \Delta I = \frac{1}{2}$ or $\Delta S = \pm 1, \Delta C = 0, \Delta I = \frac{1}{2}, \frac{3}{2}$
$\sin^2 \theta_C$	$\Delta S = -\Delta C = \pm 1, \Delta I = 0, 1$

Table XII. Examples of preferred charmed meson decay modes.

Leptonic	Γ
$F^+ \rightarrow \mu^+ \nu$	$\sim 10^9 - 10^{10} \text{ sec}^{-1}$
Semileptonic	
$D^+ \rightarrow \bar{K}^0 \ell^+ \nu$	$\sim 10^{11} - 10^{12} \text{ sec}^{-1}$
$F^+ \rightarrow \eta \ell^+ \nu$	
Hadronic	
$D^0 \rightarrow \bar{K}^0 \pi^+ + \pi^+ \pi^0$	$\sim 10^{13} \text{ sec}^{-1}$
$F^+ \rightarrow \eta \pi^+ + \pi^+ \pi^0$	

FIGURE CAPTIONS

1. e^+e^- mass spectrum from J. J. Aubert et al.⁵
2. Cross section versus total energy for (a) multihadron final states, (b) e^+e^- final states, (c) $\mu^+\mu^-$ final states. The curve in (a) is the expected shape of a δ function resonance with due account taken of beam energy spread and radiative corrections. The cross section (a), is corrected for detection efficiency whereas the cross sections (b) and (c) apply only to the detector acceptance. From J.-E. August et al.⁸
3. Relative multihadron production rate as a function of total energy. From C. Bacci et al.⁹
4. (a), (b) Fine-energy-scan data in the neighborhood of the $\psi(3095)$ and $\psi(3684)$ respectively; (c) cross section for $e^+e^- \rightarrow$ hadrons, versus total energy. The curve is the expected beam energy resolution folded with radiative corrections. From G. S. Abrams et al.¹⁰
5. Relative rates for hadron events with more than three tracks versus total energy. From L. Criegee et al.¹¹
6. (a) Spectrometer of MIT-BNL group.⁷ (b) Spectrometer of CCHF group.¹²
7. (a) DESY-DASP spectrometer.¹³ (b) SLAC-LBL Magnetic Detector.¹⁴
8. Cross sections for the production by e^+e^- of (a) collinear photon pairs, (b) non-collinear photon pairs, from W. Braunschweig et al.¹⁵
(c) Observed $e^+e^- \rightarrow 2\gamma$ rate as a function of energy per beam from R. L. Ford et al.¹⁶
9. Cross sections for (a) $e^+e^- \rightarrow$ hadrons, (b) $e^+e^- \rightarrow \mu^+\mu^-$ and (c) $e^+e^- \rightarrow e^+e^-$ versus total energy, in the neighborhood of $\psi(3095)$ from A. M. Boyarski et al.¹⁸
10. Cross sections for (a) $e^+e^- \rightarrow$ hadrons, (b) $e^+e^- \rightarrow \mu^+\mu^-$ and (c) $e^+e^- \rightarrow e^+e^-$ versus total energy in the neighborhood of $\psi(3684)$ from V. Lüth et al.¹⁹
11. Diagrams for hadron and $\mu^+\mu^-$ production in annihilation (a) direct ψ decay to hadrons, (b) ψ decay to hadrons via intermediate photon,

- (c) off-resonance annihilation to hadrons, (d) ψ decay to $\mu^+\mu^-$ via intermediate photon, (e) off-resonance annihilation to $\mu^+\mu^-$.
12. Forward-backward asymmetry in $e^+e^- \rightarrow \mu^+\mu^-$ as a function of energy in (a) neighborhood of $\psi(3095)$, (b) neighborhood of $\psi(3684)$, from SLAC-LBL. ^{18,19}
 13. Energy dependence of ratio of $\sigma(e^+e^- \rightarrow \mu^+\mu^-)/\sigma(e^+e^- \rightarrow e^+e^-)$ in the neighborhood of (a) $\psi(3095)$, (b) $\psi(3684)$, from SLAC-LBL. ^{18,19}
 14. Angular distributions for (a) $e^+e^- \rightarrow e^+e^-$ and (b) $e^+e^- \rightarrow \mu^+\mu^-$ near peak of $\psi(3095)$, from A. M. Boyarski et al. ¹⁸
 15. Invariant mass distribution of $\mu^+\mu^-$ of energy greater than 70 GeV, produced by incident neutrons, from B. Knapp et al. ²⁴
 16. Invariant mass distribution of e^+e^- produced in pp collisions of the ISR. The curves indicate the shapes of the acceptance, from F. W. Büsler et al. ²⁵
 17. x and P_{\perp} distributions for $\psi(3095)$ production by 200 GeV protons and π^- on iron, from G. J. Blunar et al. ²⁶
 18. Photoproduction of $\psi(3095)$ on beryllium at 11.8 GeV, from B. Gittelman et al. ²⁸
 19. Photoproduction of $\psi(3095)$ on beryllium at 100-200 GeV, from B. Knapp et al. ¹²
 20. Energy dependence of forward photoproduction cross section of $\psi(3095)$, from compilation by B. Gittelman et al. ²⁸
 21. M_X^2 distribution for $e^+e^- \rightarrow 2\pi^+2\pi^-X$ (a) at 3.0 GeV and (b) for $\psi(3095)$, from A. M. Boyarski et al. ³⁰
 22. Plot of ratio α (defined in text) versus multiplicity for $\psi(3095)$ from A. M. Boyarski et al. ³⁰
 23. Dalitz plot for $\psi(3095) \rightarrow \pi^+\pi^-\pi^0$ from A. M. Boyarski et al. ³⁰
 24. Momentum of Λ versus momentum of $\bar{\Lambda}$ in reaction $\psi(3095) \rightarrow \Lambda\bar{\Lambda} + \text{anything}$, from A. M. Boyarski et al. ³⁰
 25. $\pi^+\pi^-\pi^0$ effective mass distribution from $\psi(3095) \rightarrow 2\pi^+2\pi^-\pi^0$, from SLAC-LBL data (unpublished).

26. Momentum of positive lepton versus momentum of negative lepton for near-collinear 2-prong events from $\psi(3684)$. Dashed lines indicate cuts used to select direct decays of $\psi(3684)$, from V. Lüth et al.¹⁹
27. (a) Inclusive $\mu^+\mu^-$ mass spectrum from $\psi(3684)$. (b) Missing mass distribution recoiling against $\pi^+\pi^-$. (c) Same as (b) for 4-prong, $Q = 0$ events with missing momentum and energy compatible with zero, from G. S. Abrams et al.³⁴
28. $\pi^+\pi^-$ mass spectrum from $\psi(3684) \rightarrow \pi^+\pi^-\psi(3095)$. The curve is a phase space distribution corrected by the acceptance, from J. A. Kadyk et al.³⁵
29. Spectrum of missing mass recoiling against $\psi(3095)$ for events of the type $\psi(3684) \rightarrow \psi(3095) + \text{neutrals}$, $\psi(3095) \rightarrow \mu^+\mu^-$, from W. Tanenbaum et al.⁴⁶
30. Scatter plots of missing momentum versus total observed energy for zero charge, 4-prong events. (a) $\psi(3095) \rightarrow \text{anything}$, (b) $\psi(3684) \rightarrow \text{anything}$, (c) $\psi(3684) \rightarrow \pi^+\pi^-\psi(3095)$, (d) $\psi(3684) \not\rightarrow \pi^+\pi^-\psi(3095)$. From A. M. Boyarski et al.³⁰
31. $\sigma(e^+e^- \rightarrow \text{hadrons})$ and R versus total energy, from G. J. Feldman.³⁸
32. Inclusive photon energy spectra produced in $\psi(3684)$ decay; (a) converted events, (b) unconverted events, from J. W. Simpson et al.⁴³
33. $p\bar{p}$ mass spectra produced in P-Be collisions from J. J. Aubert et al.^{6,48}
34. $K^+\pi^-$ mass spectra from J. J. Aubert et al.^{6,48}
35. Invariant mass spectra for various particle hypotheses at a total energy of 4.8 GeV, from A. M. Boyarski et al.⁵¹

00004402596

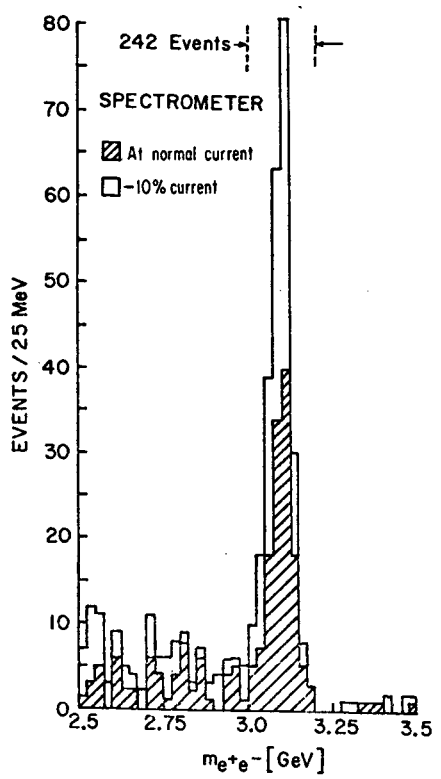


Fig. 1

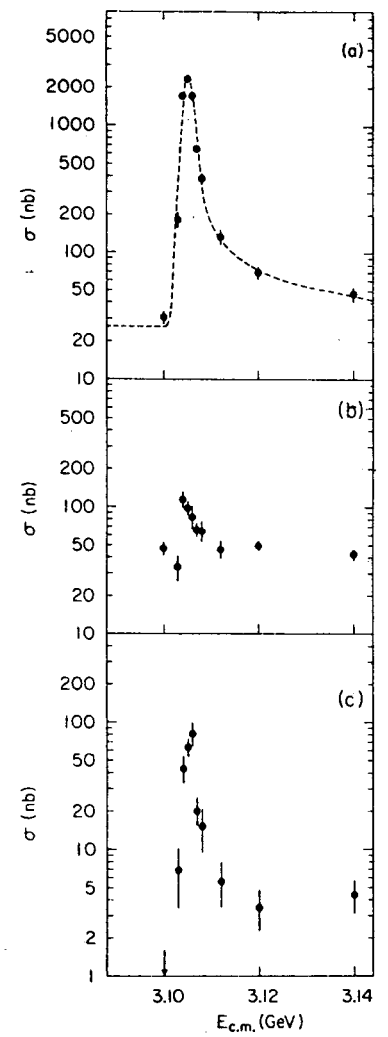


Fig. 2

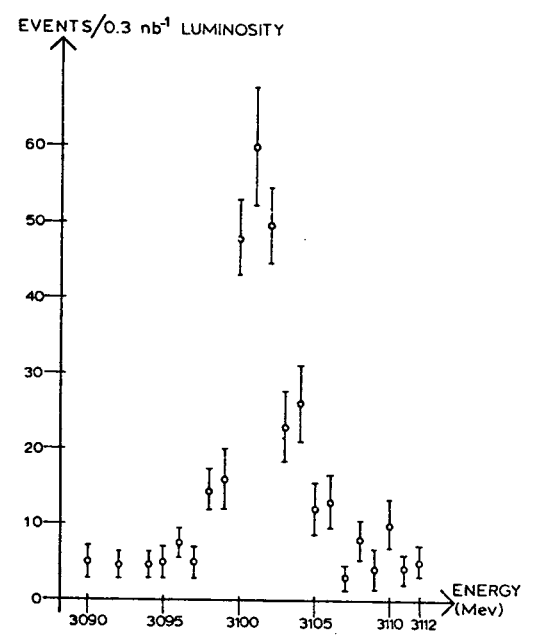


Fig. 3

XBL 7510-8476

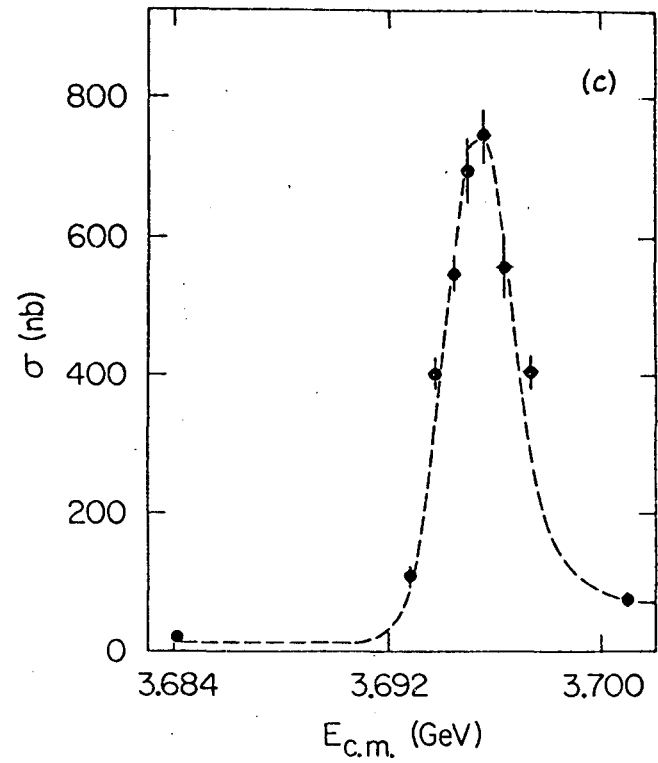
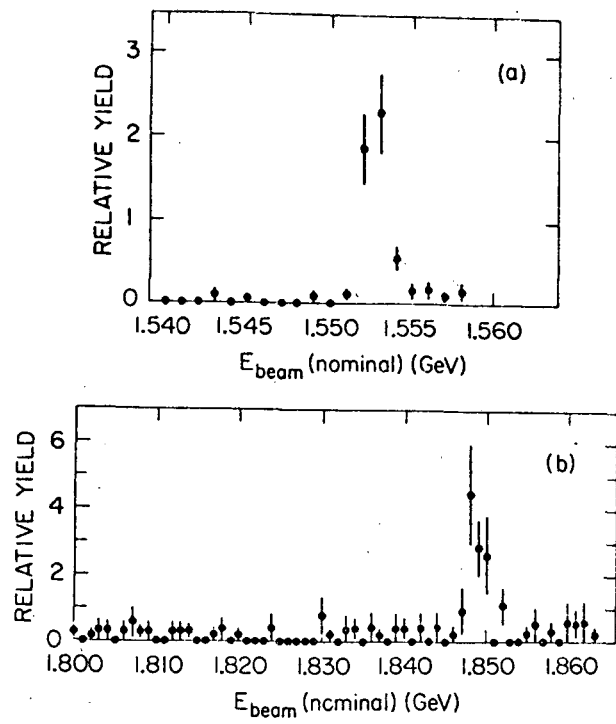


Fig. 4

XBL 7510-8467

00004402597

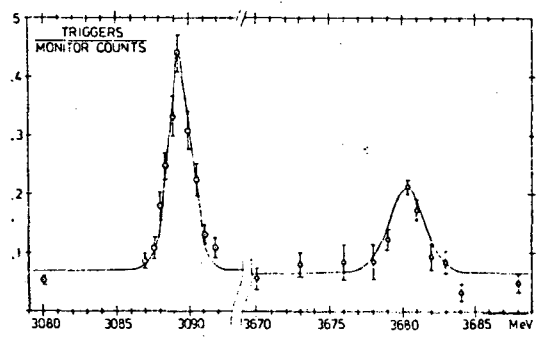
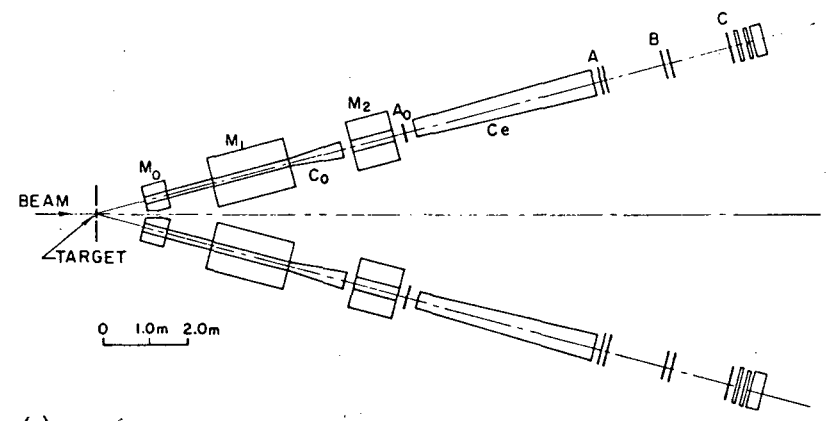


Fig. 5



(a)

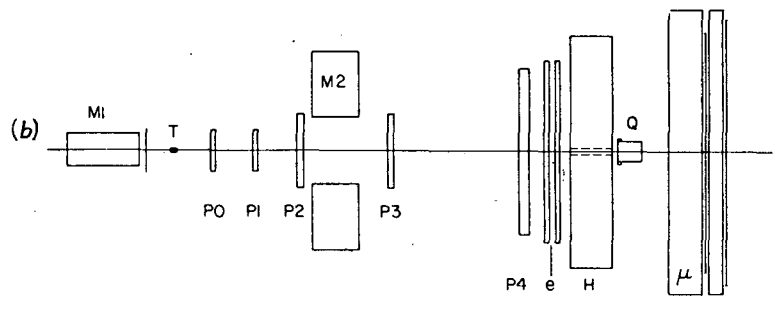
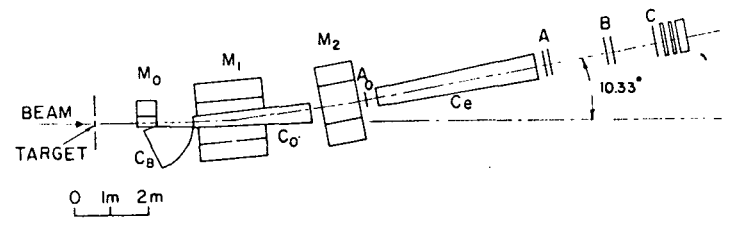


Fig. 6

XBL 7510-8475

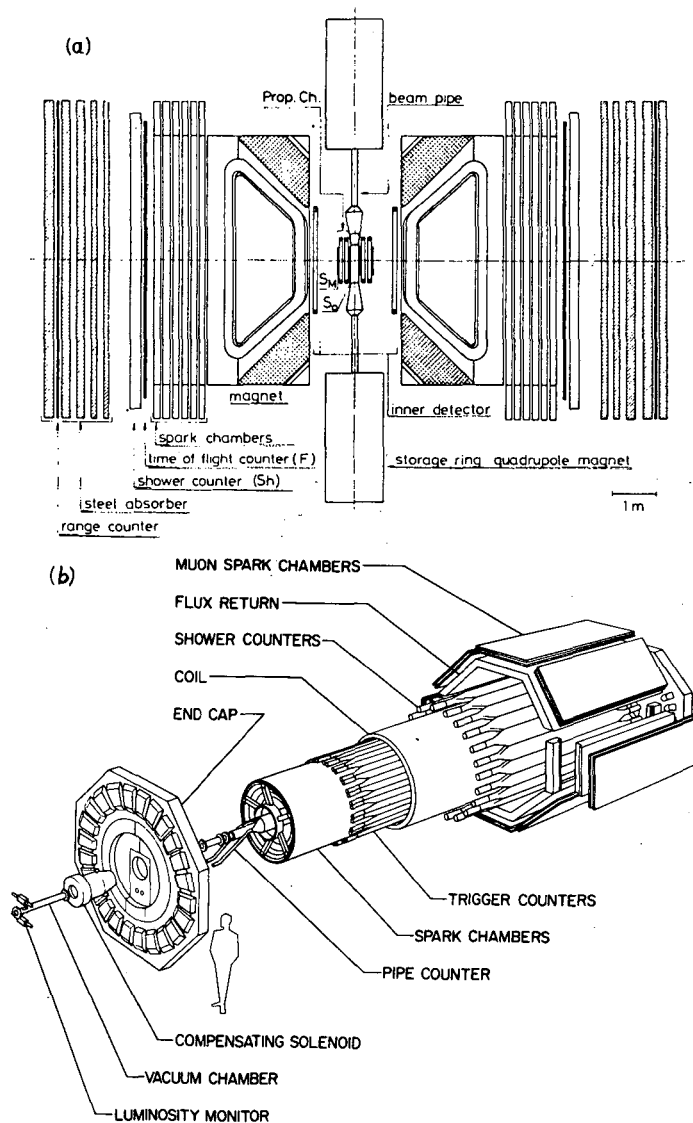


Fig. 7

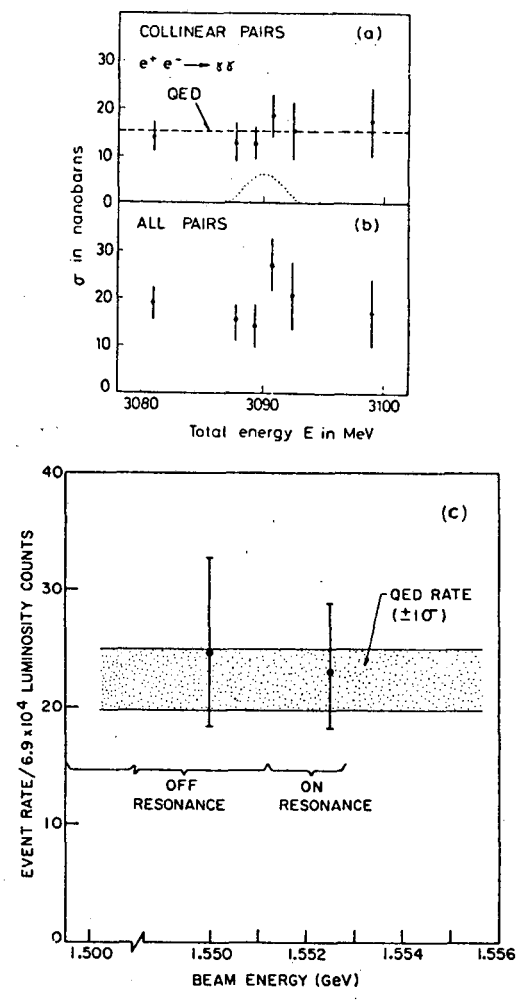


Fig. 8

XBL 7510-8474

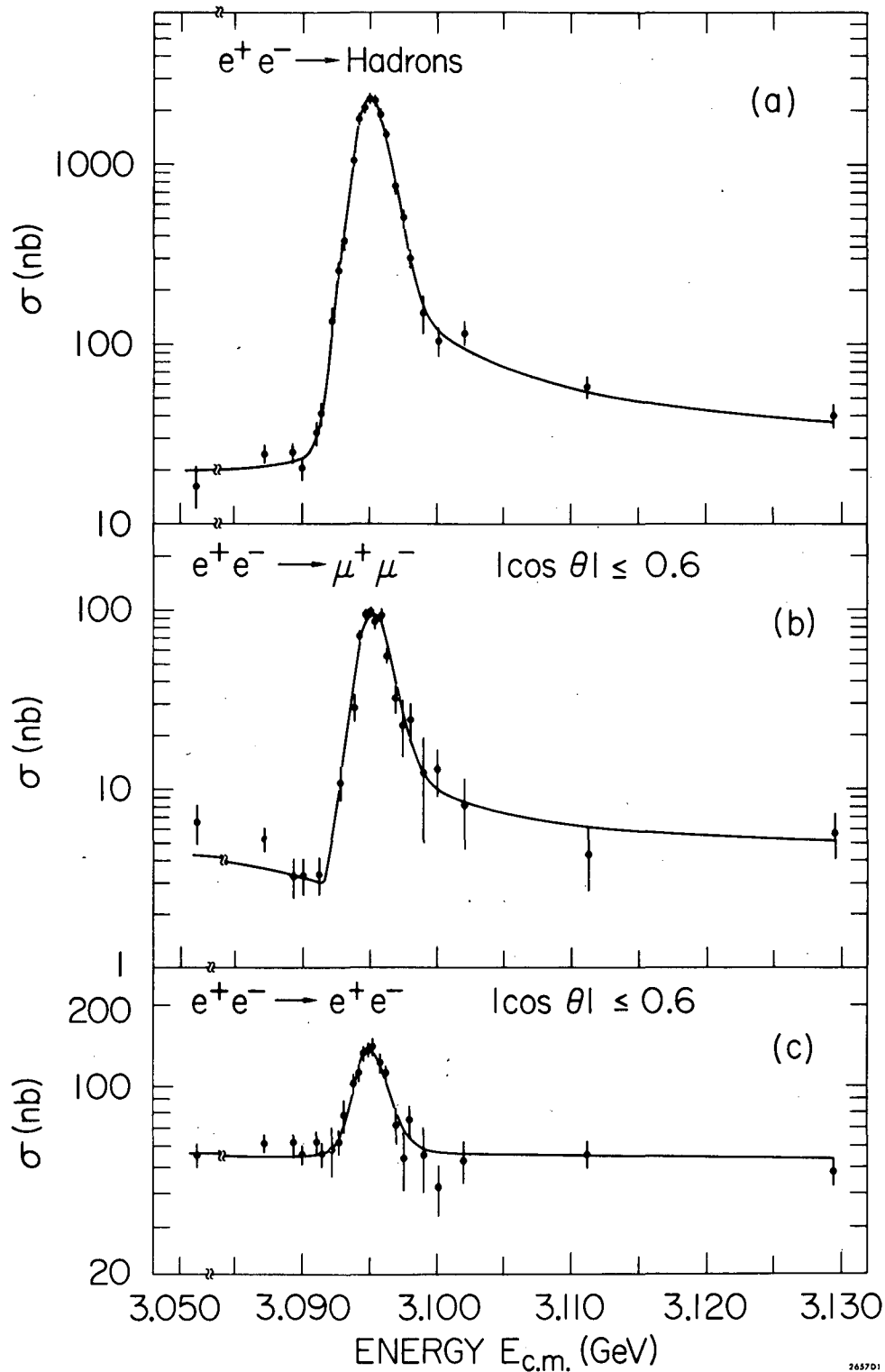


Fig. 9

0 0 0 0 4 4 0 2 5 9 8

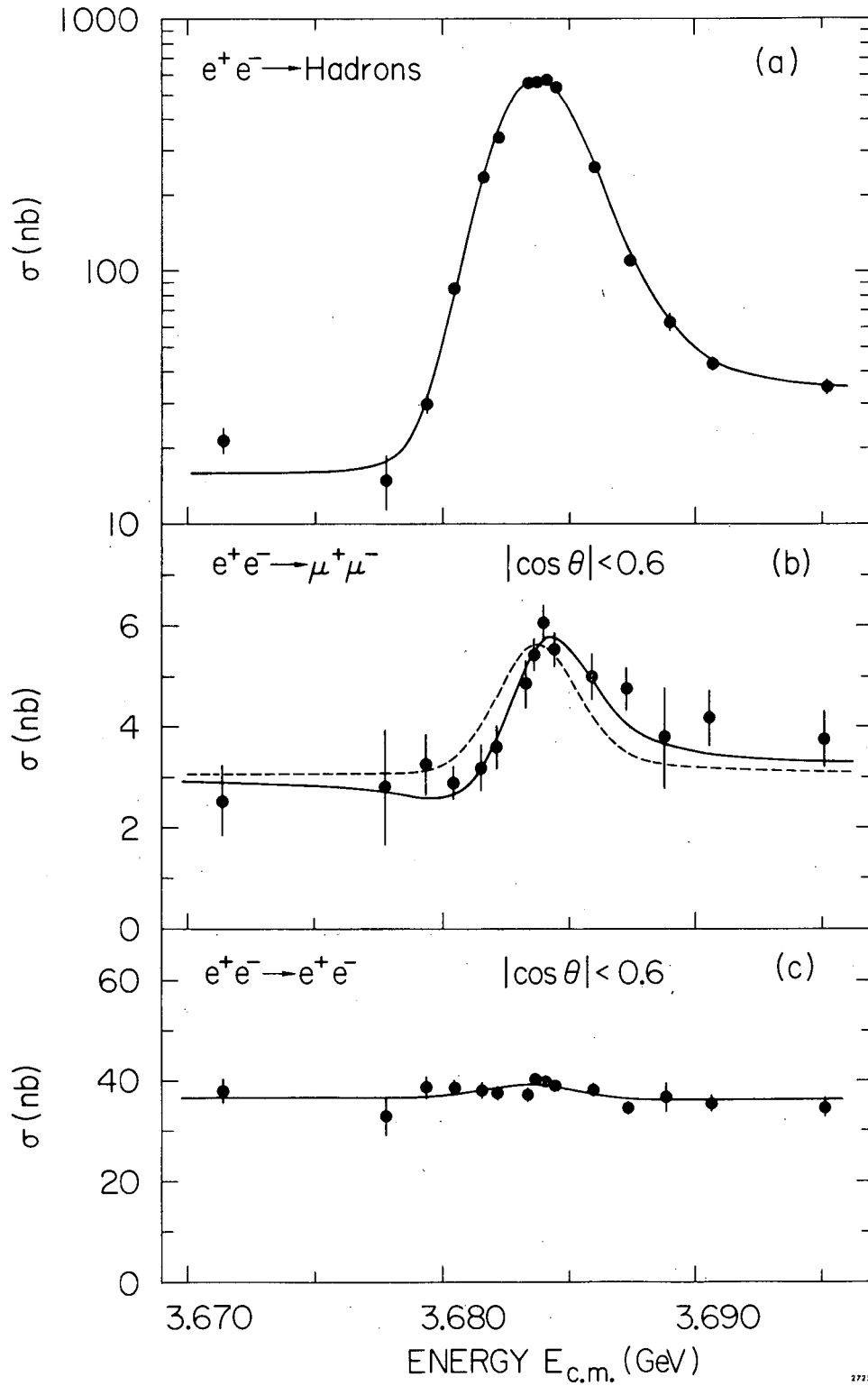


Fig. 10

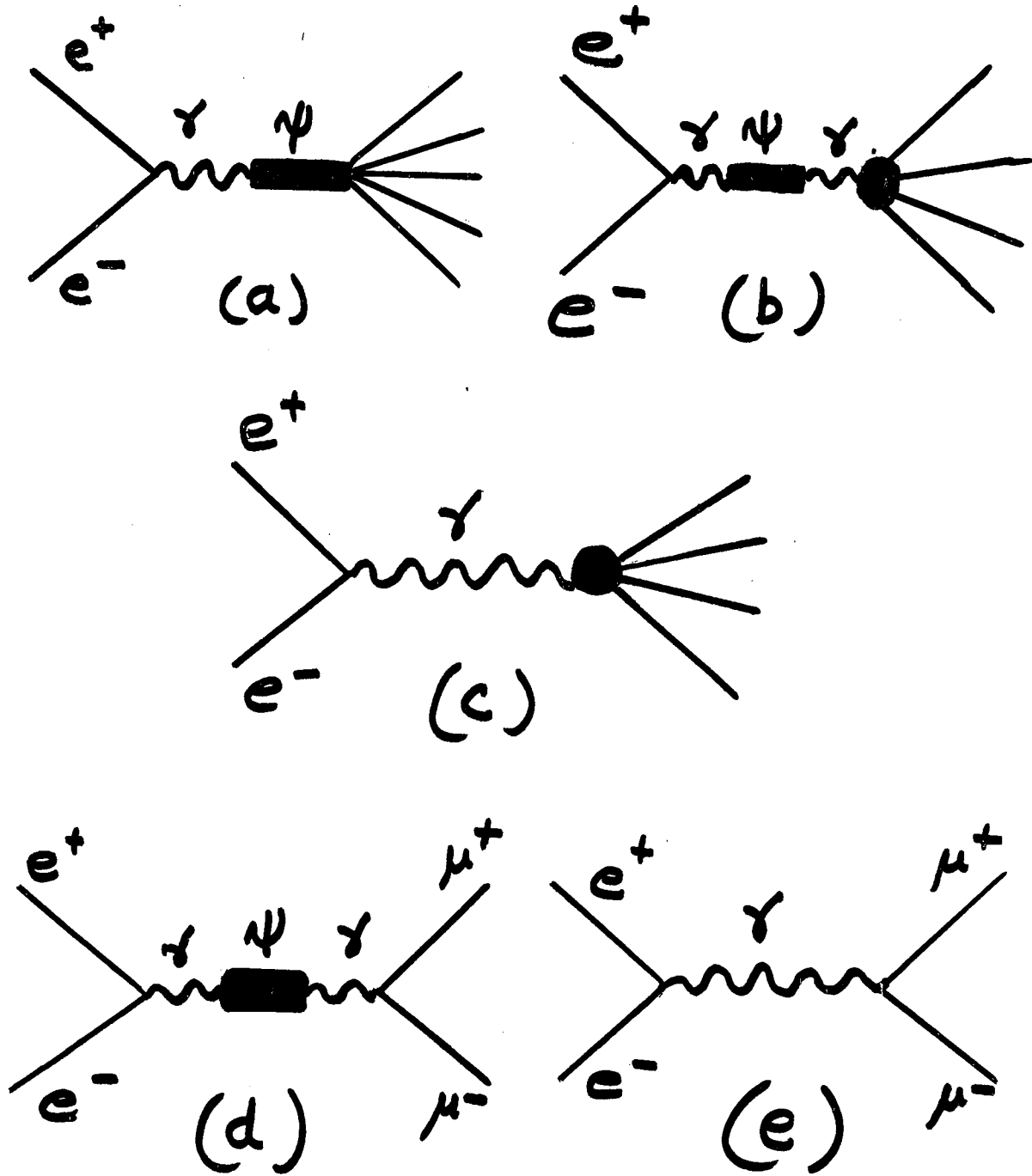


Fig. 11

XBL 7510-8473

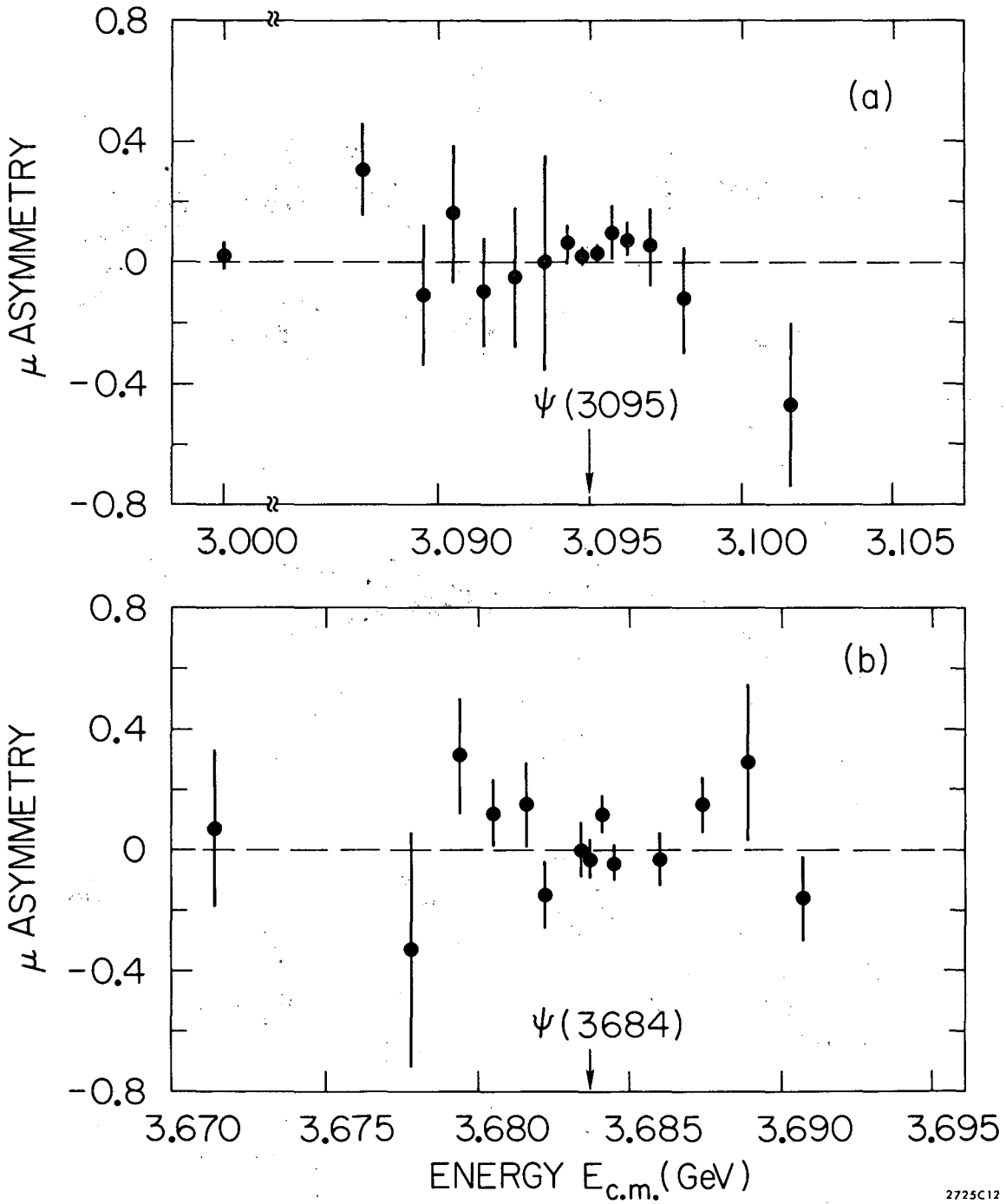


Fig. 12

2725C12

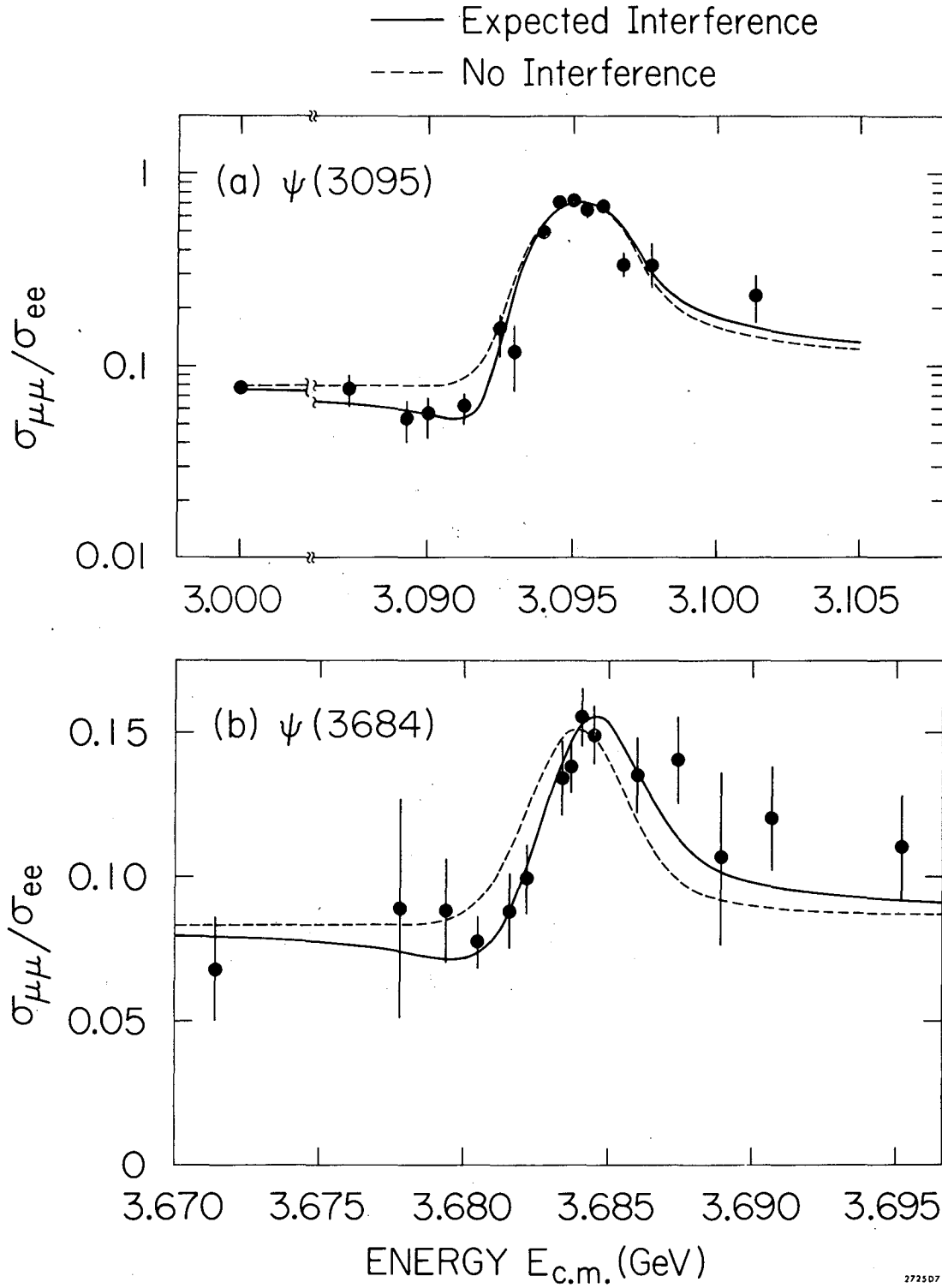


Fig. 13

0 0 9 2 0 4 4 0 0 0 0

2725D7

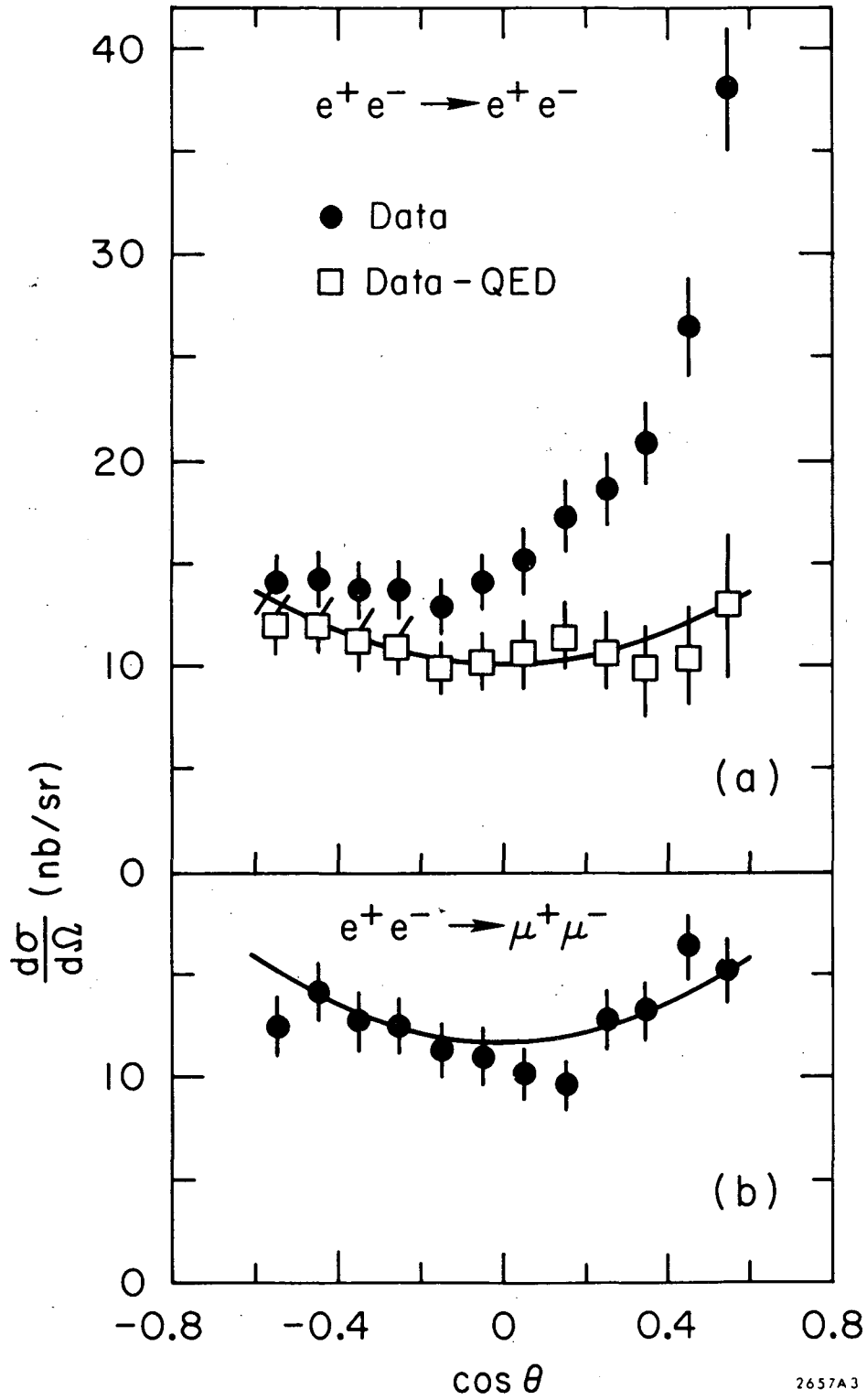


Fig. 14

2657A3

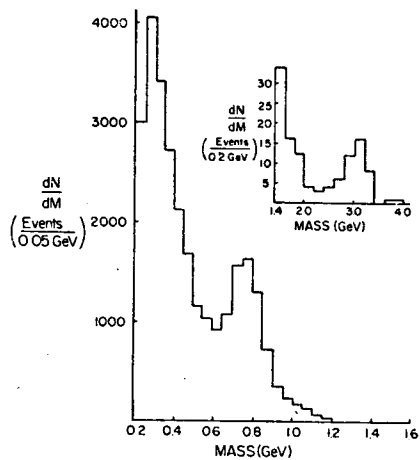


Fig. 15

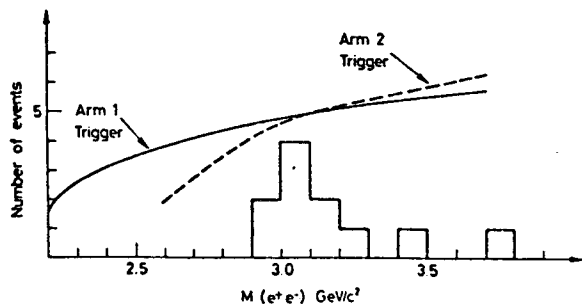


Fig. 16

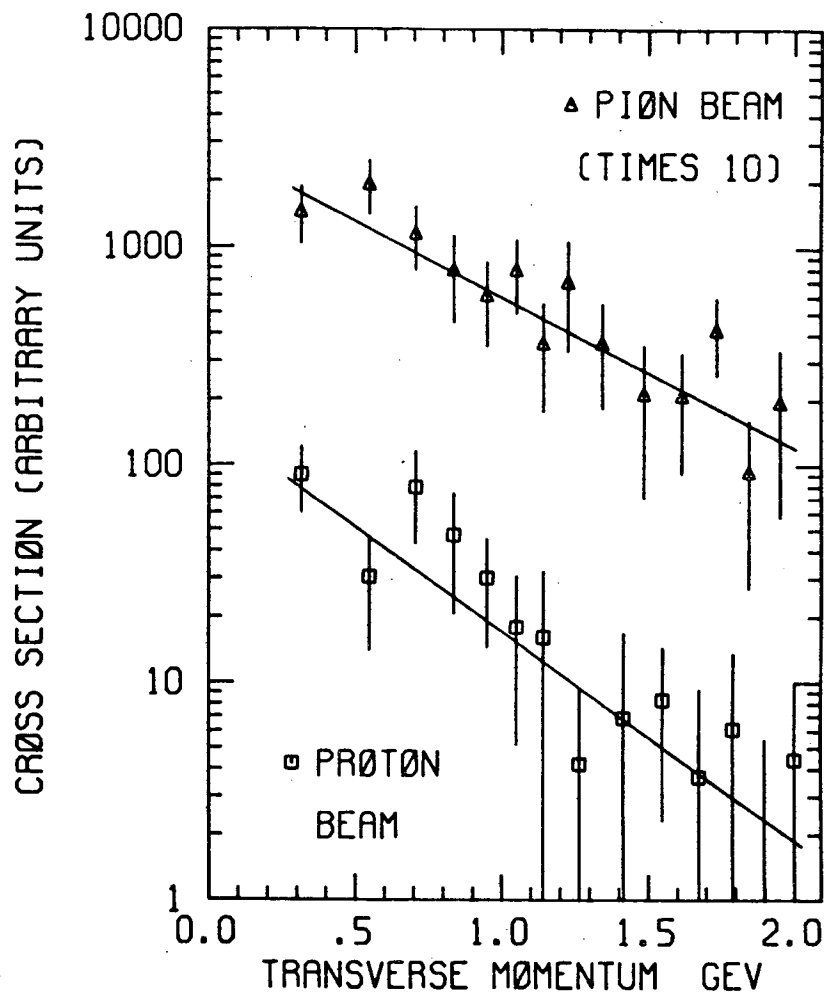


Fig. 17

XBL 7510-8472

00004402601

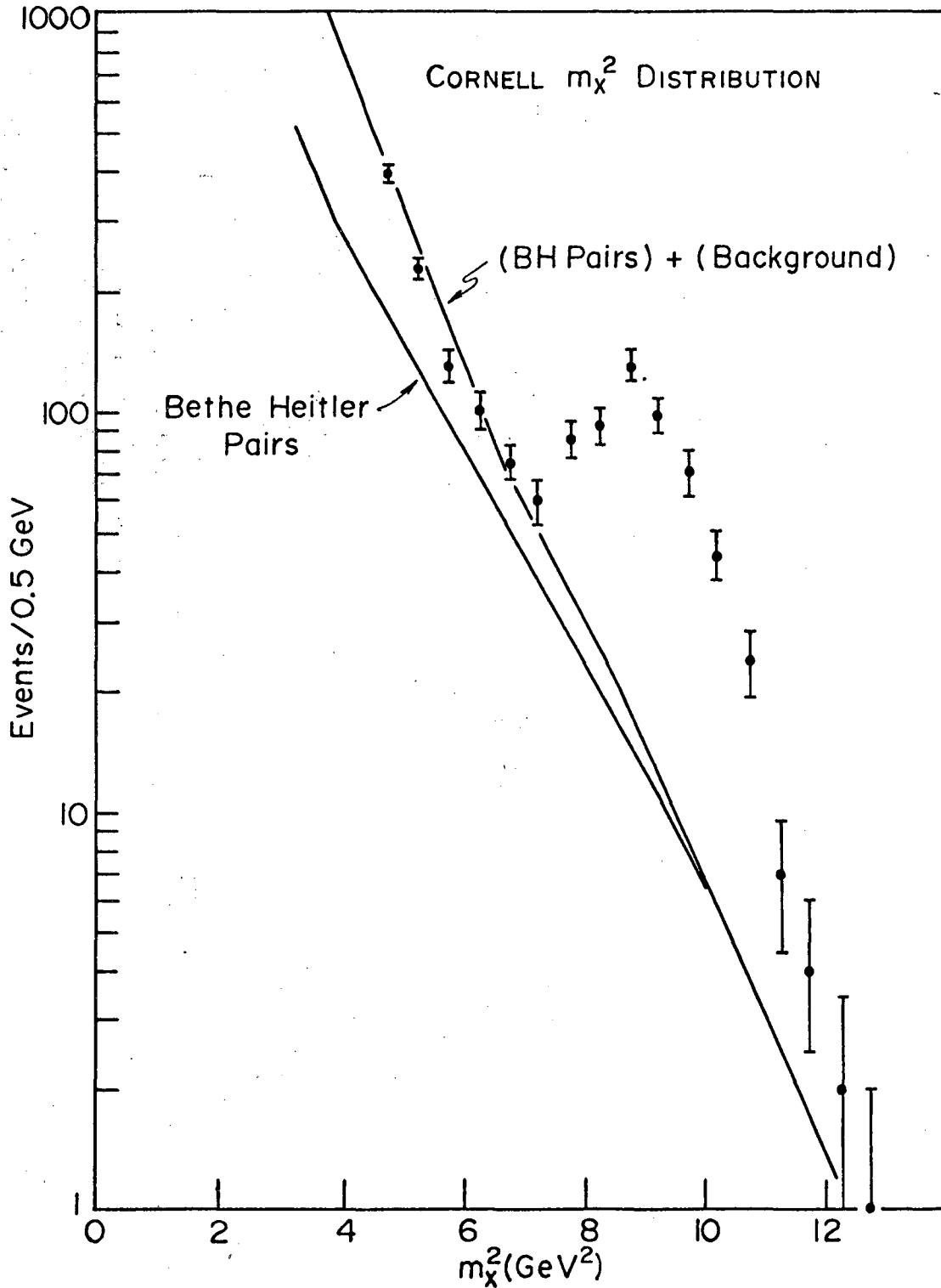


Fig. 18

XBL 7510-8468

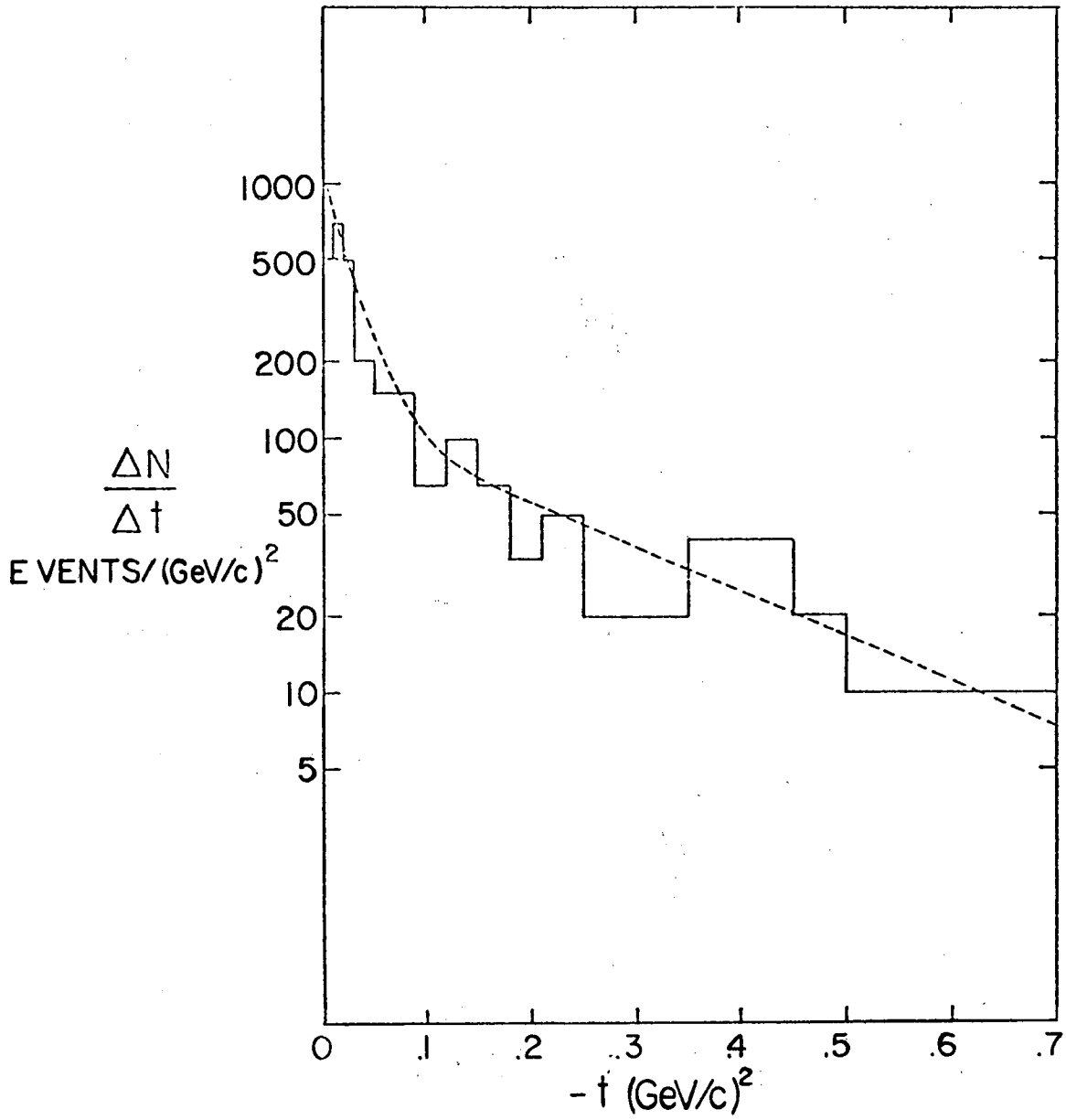


Fig. 19

XBL 7510-8469

0 0 0 0 4 4 0 2 6 0 2

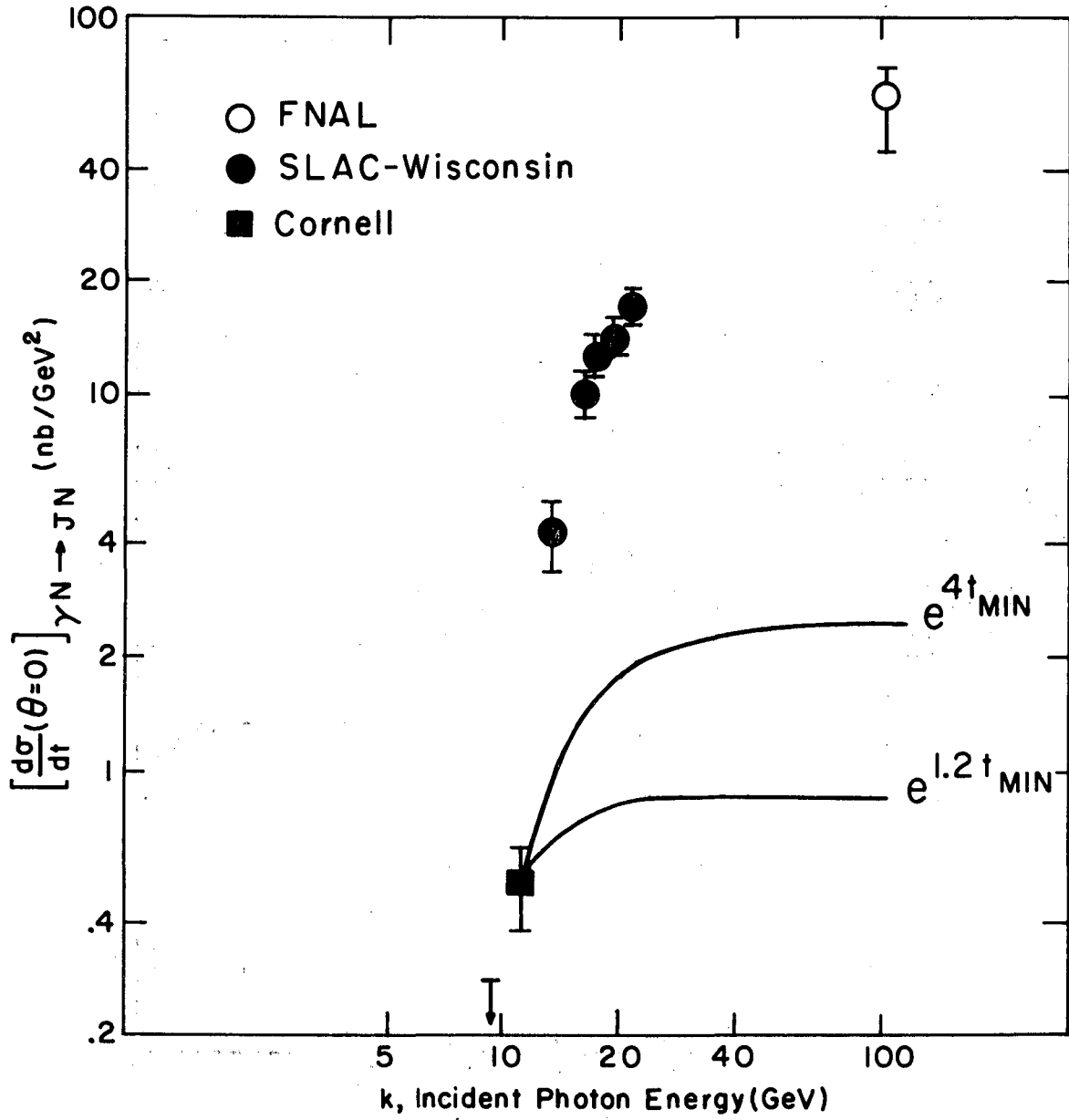


Fig. 20

XBL 7510-8470

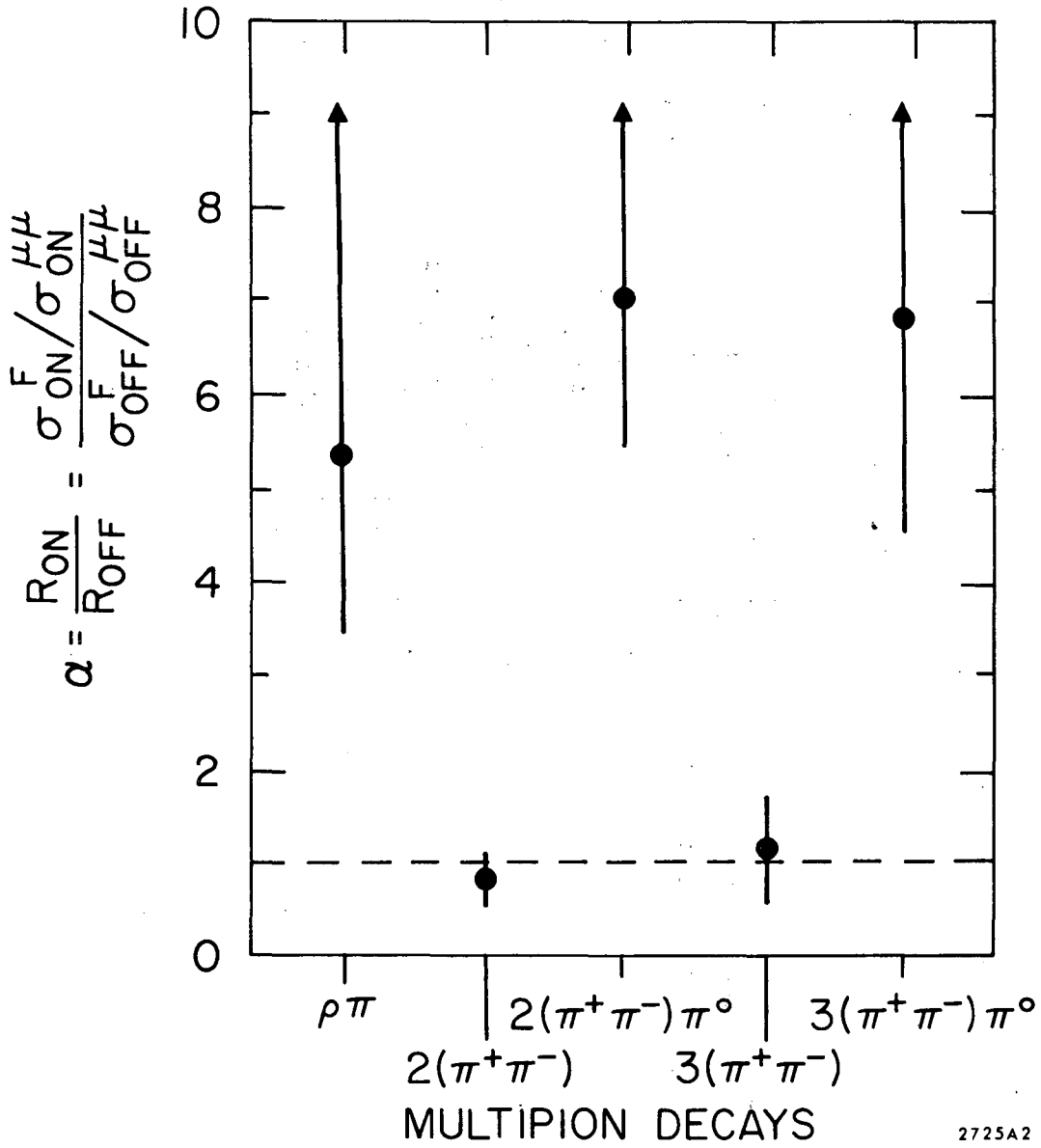


Fig. 22

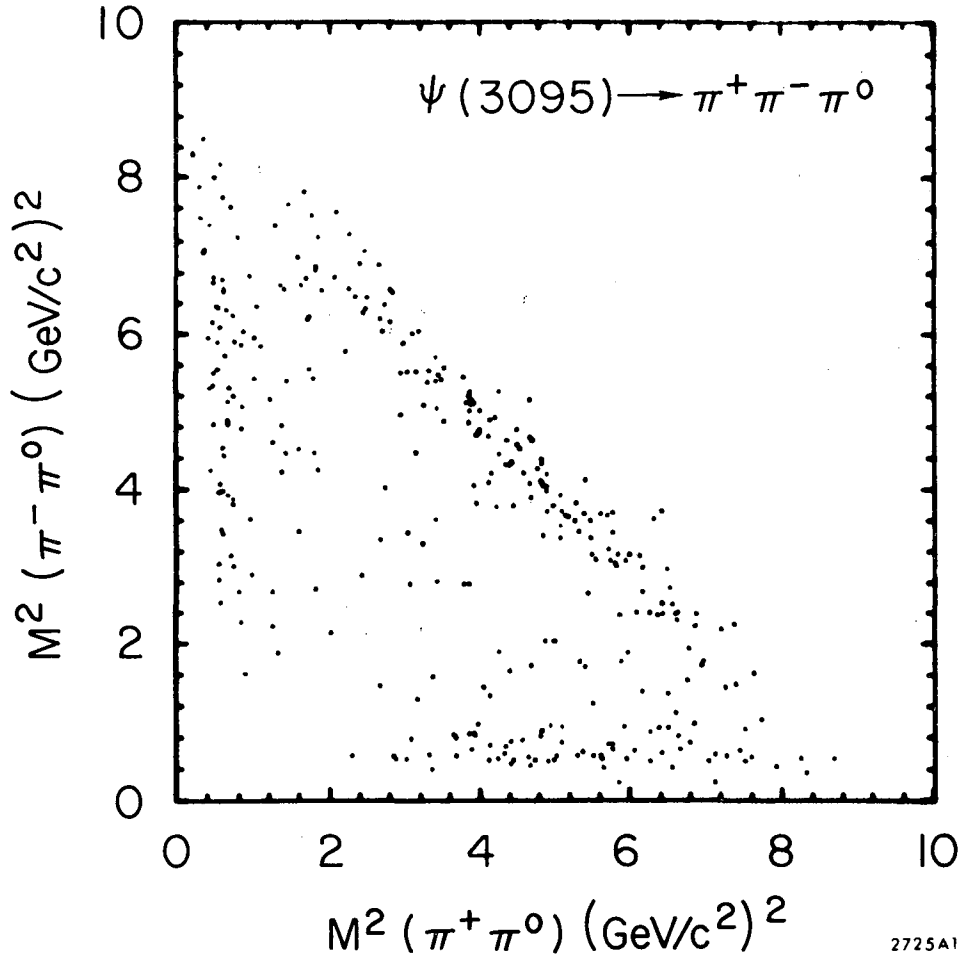


Fig. 23

00004402604

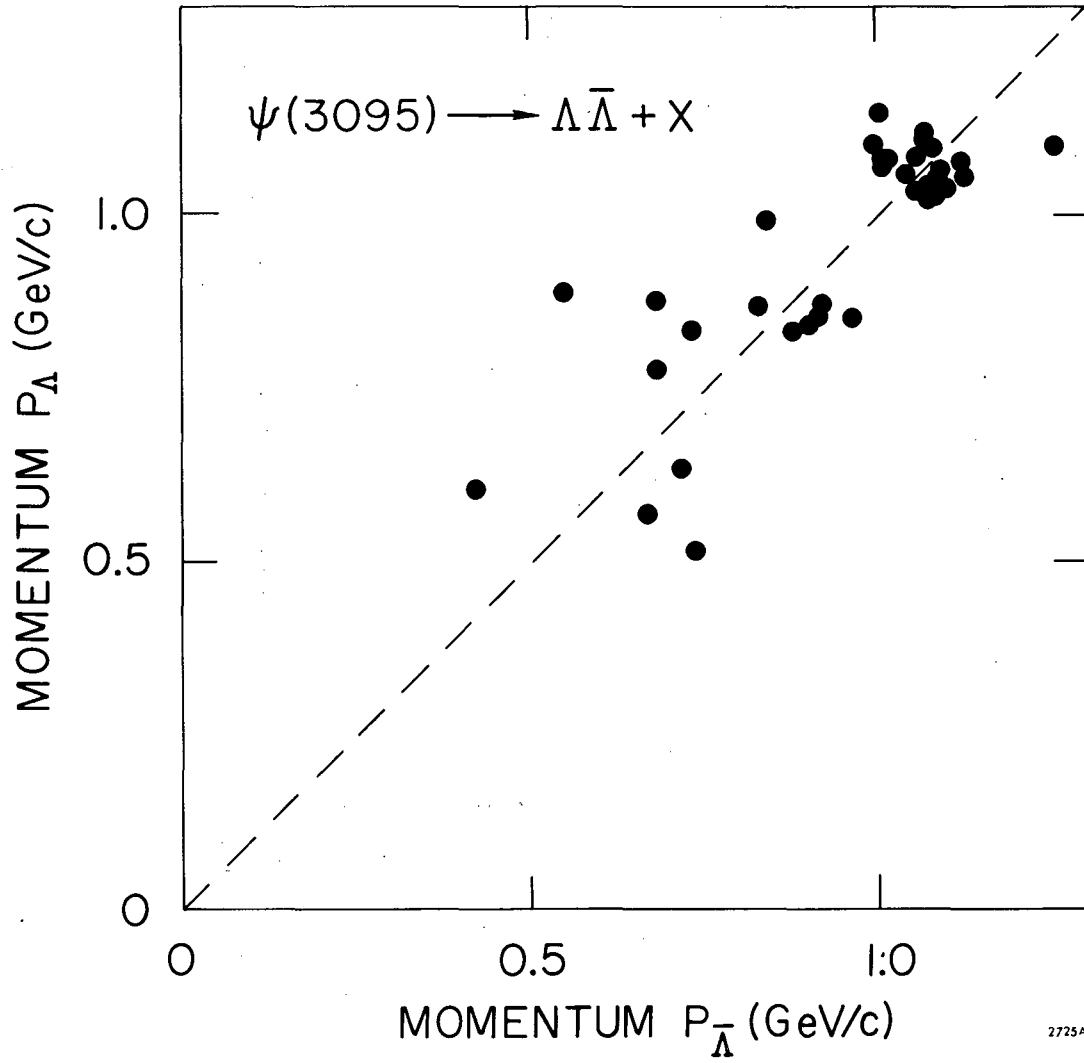


Fig. 24

2725A21

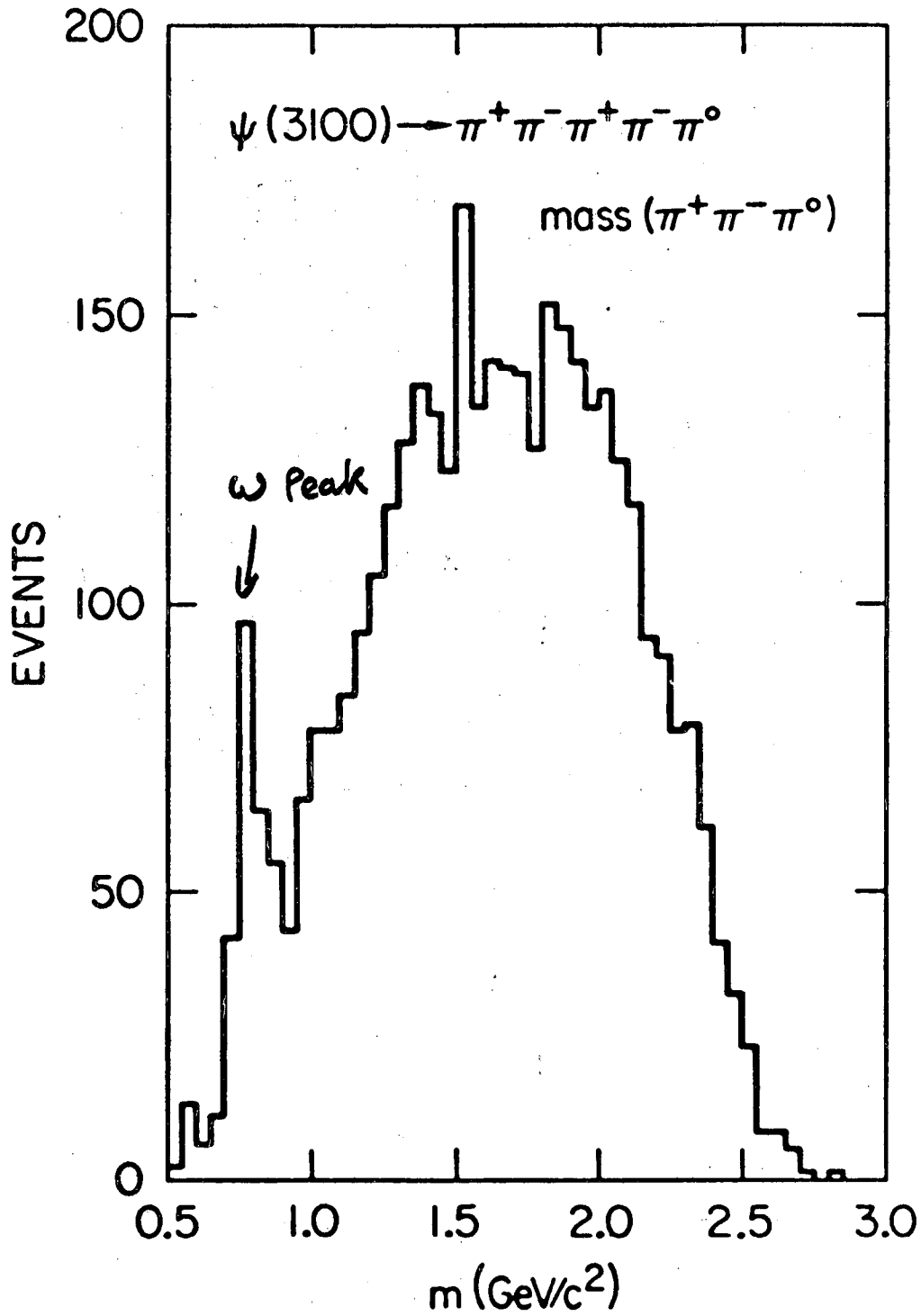


Fig. 25

XBL 7510-8471

5 0 9 7 0 7 4 0 0 0 0

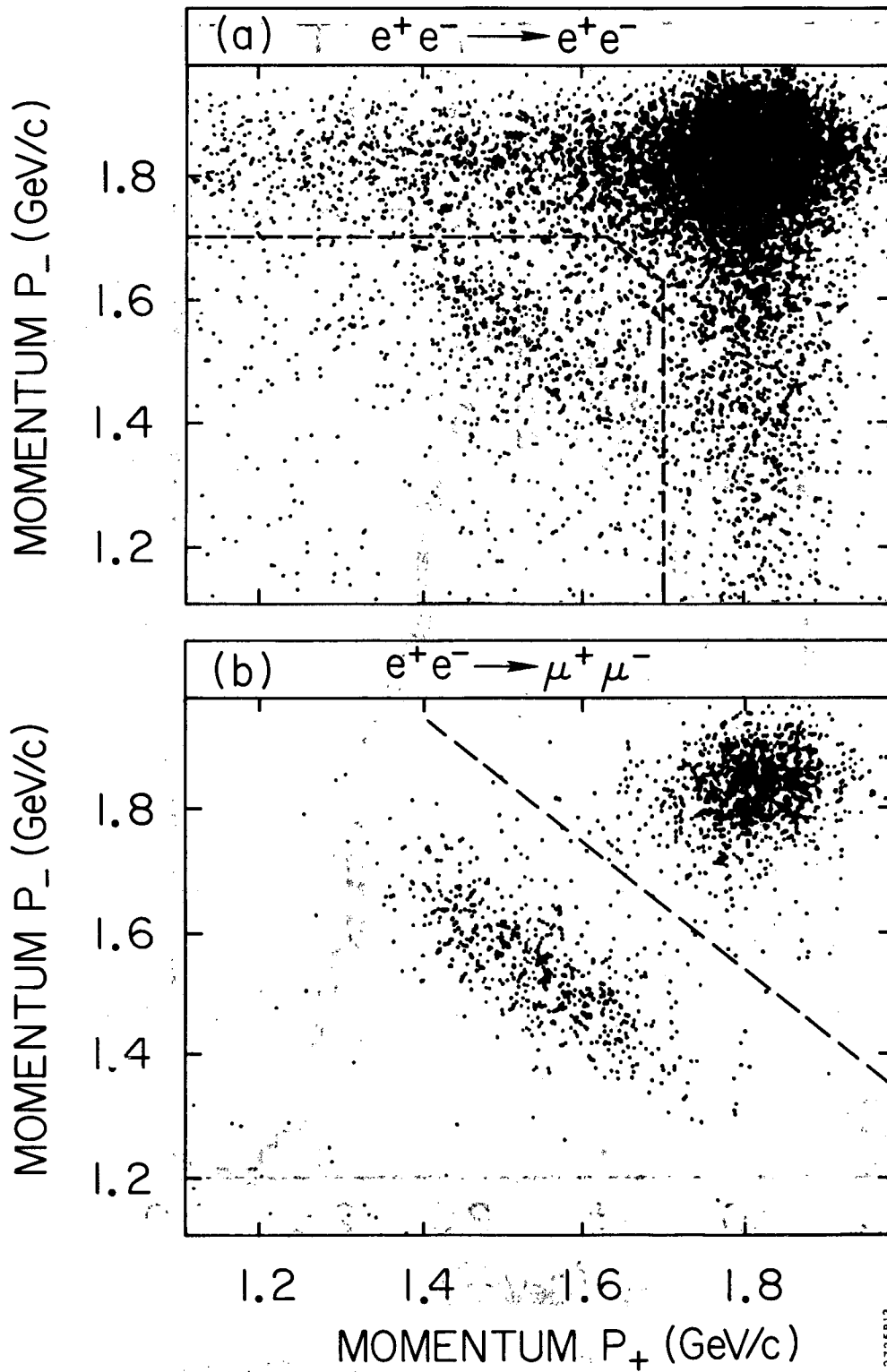


Fig. 26

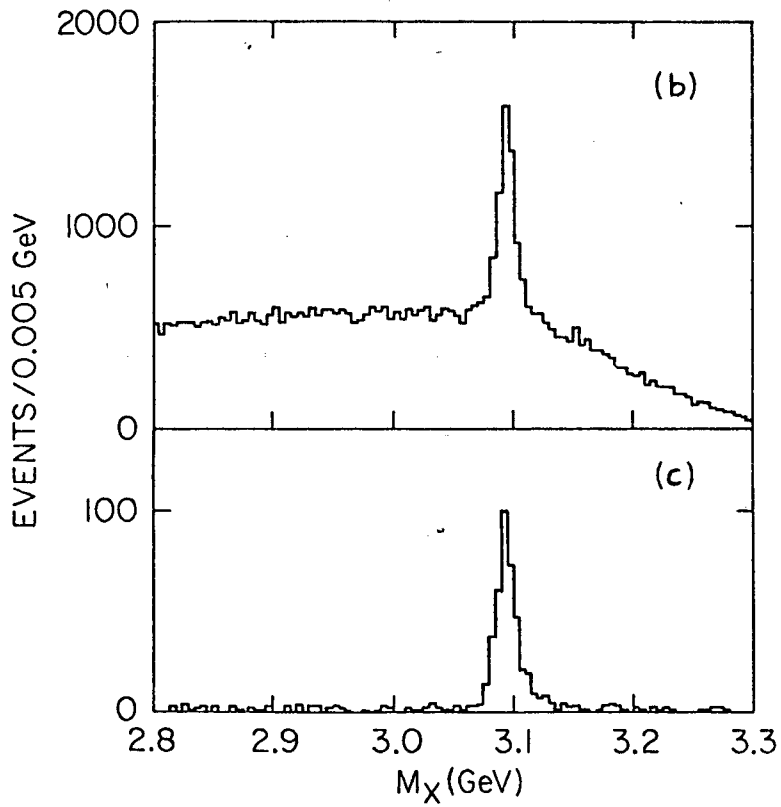
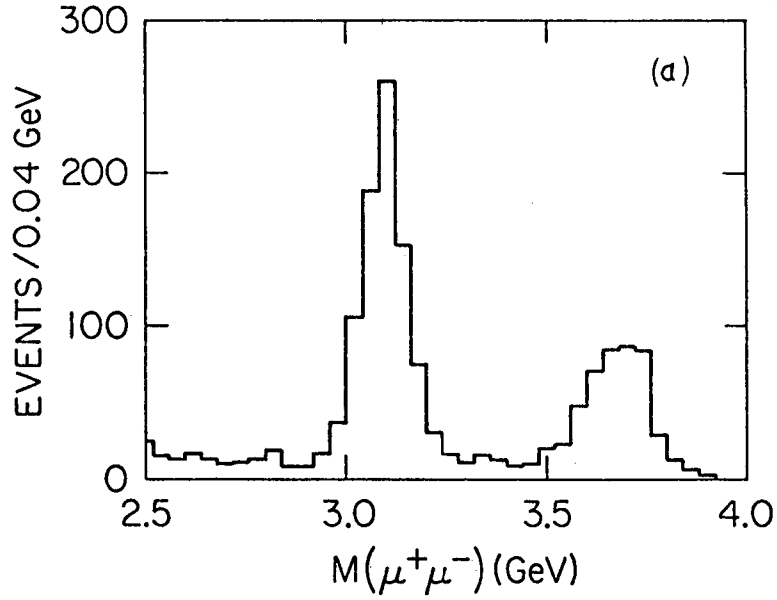


Fig. 27

XBL 7510-8477

00004402609

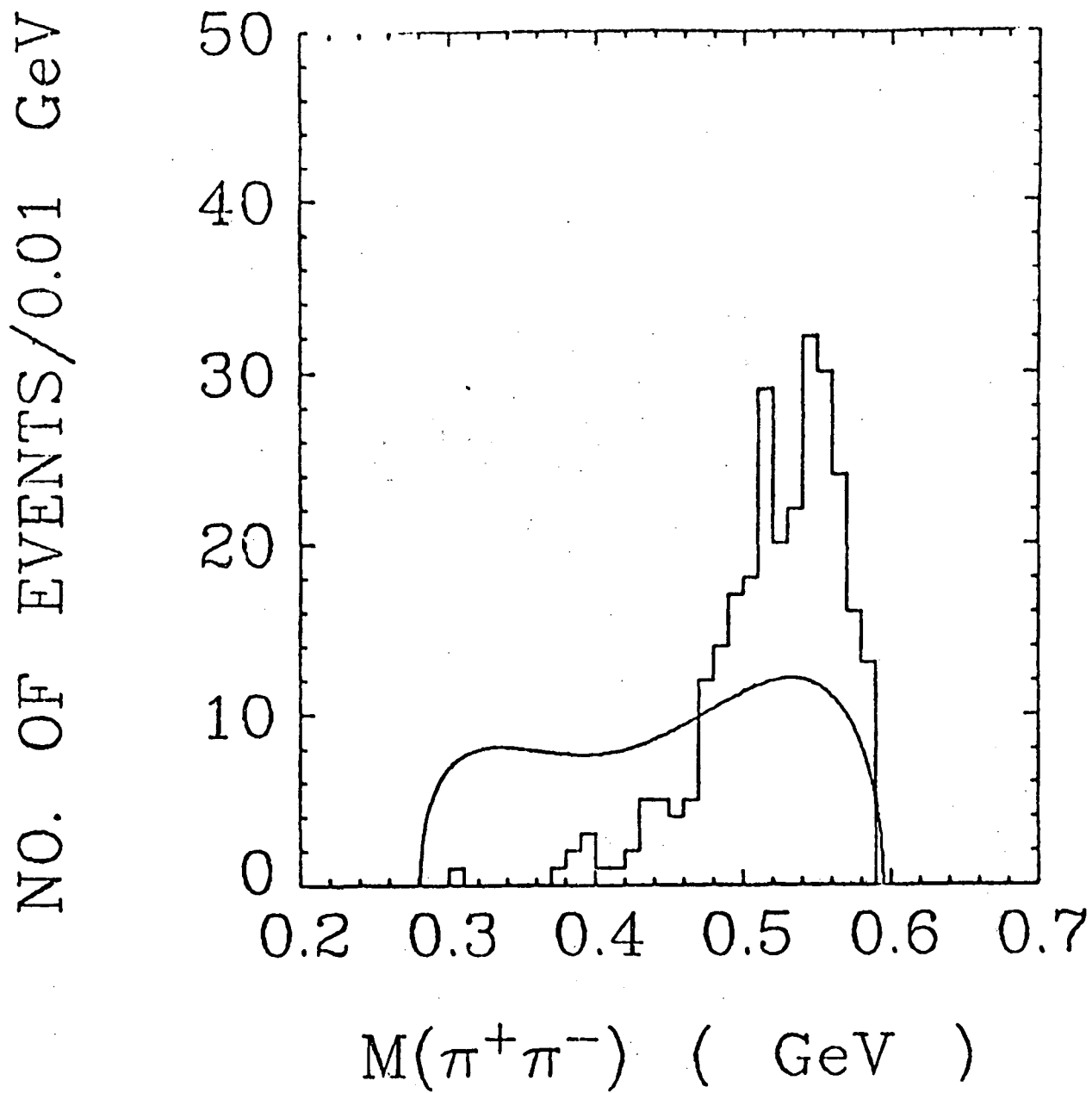


Fig. 28

XBL 753-531

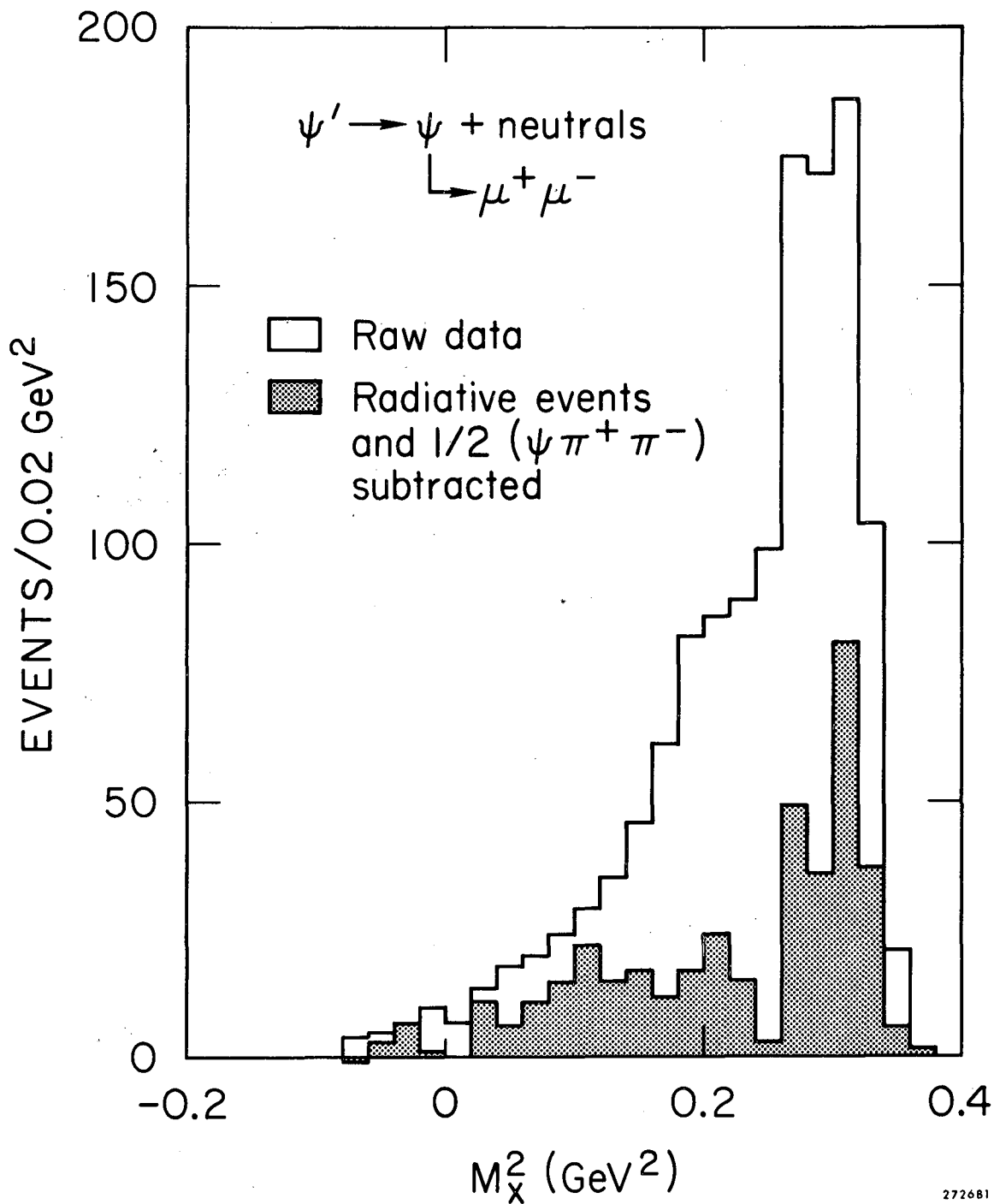


Fig. 29

0 0 0 0 4 4 0 2 6 0 7

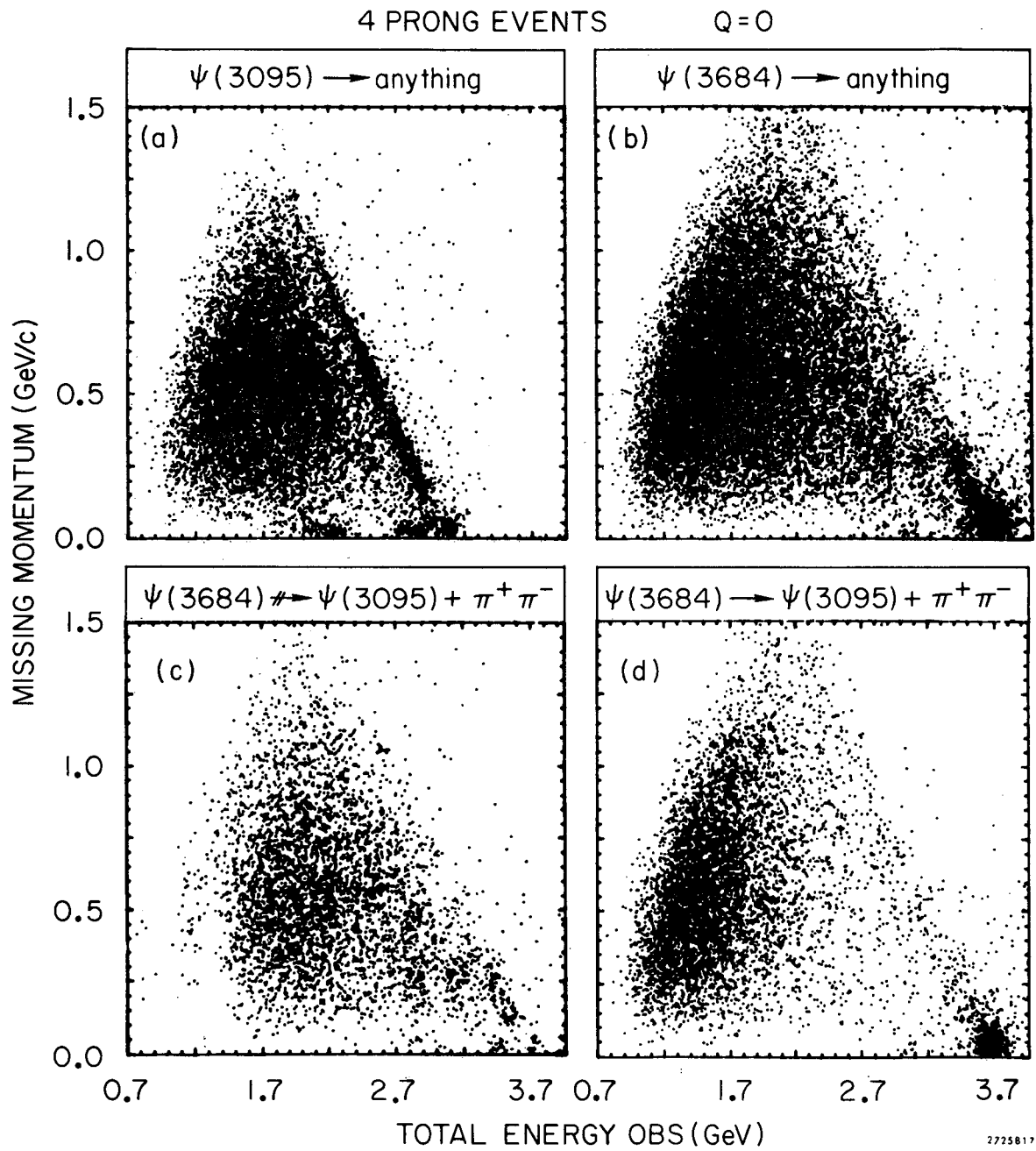


Fig. 30

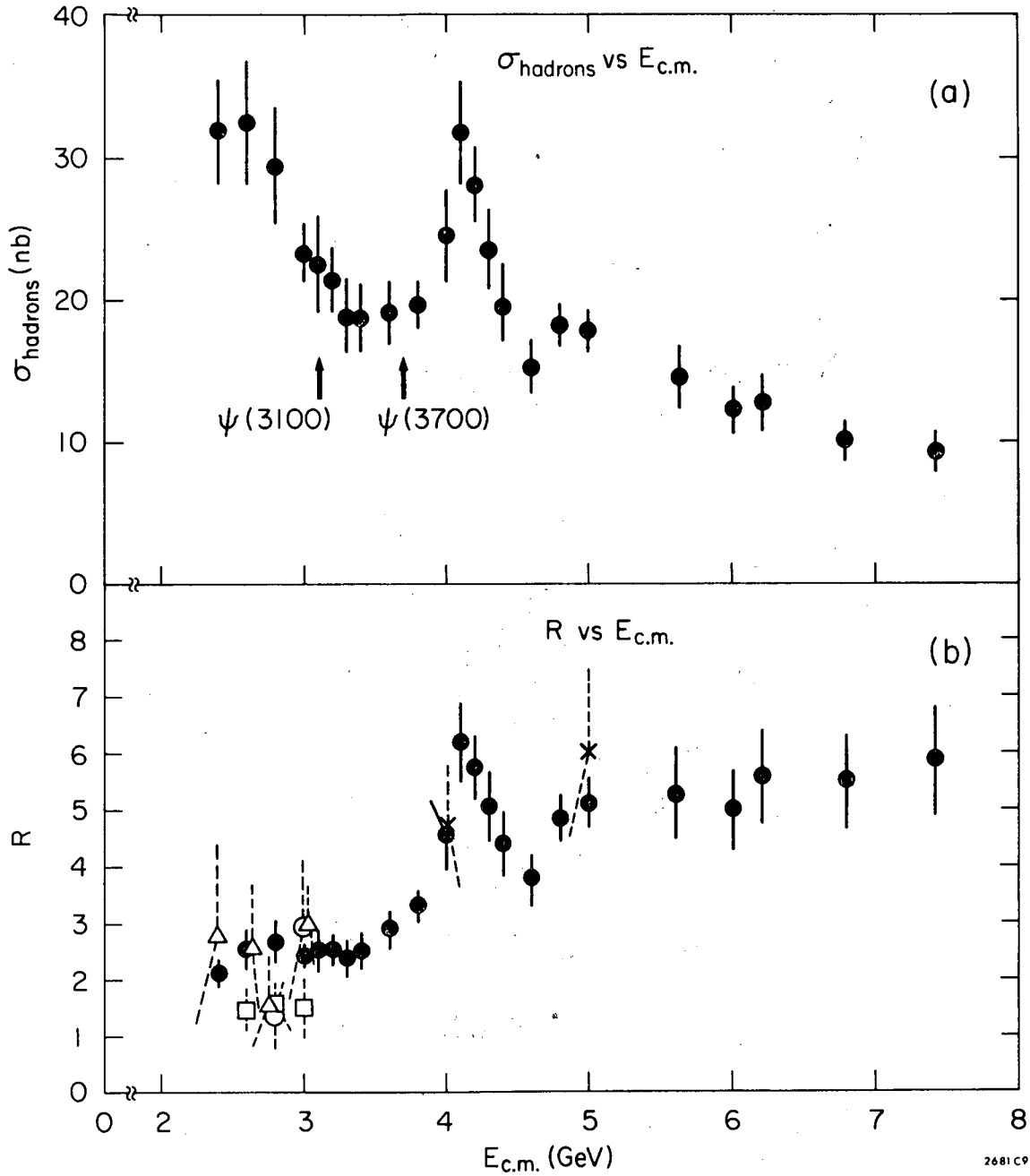


Fig. 31

0 0 0 0 4 4 0 2 6 0 8

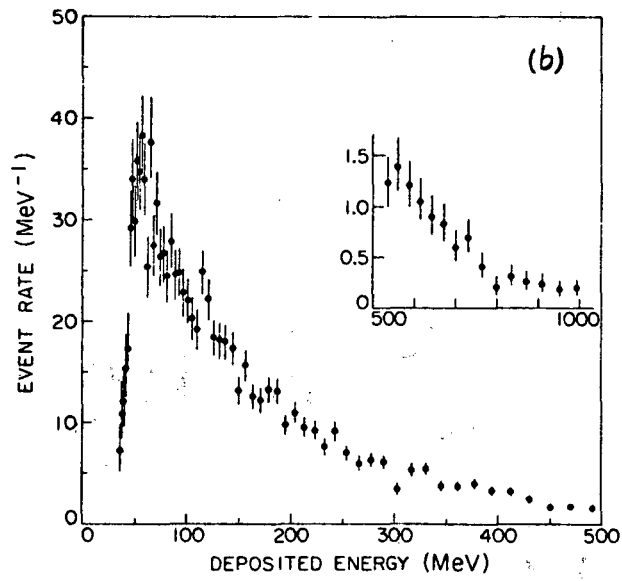
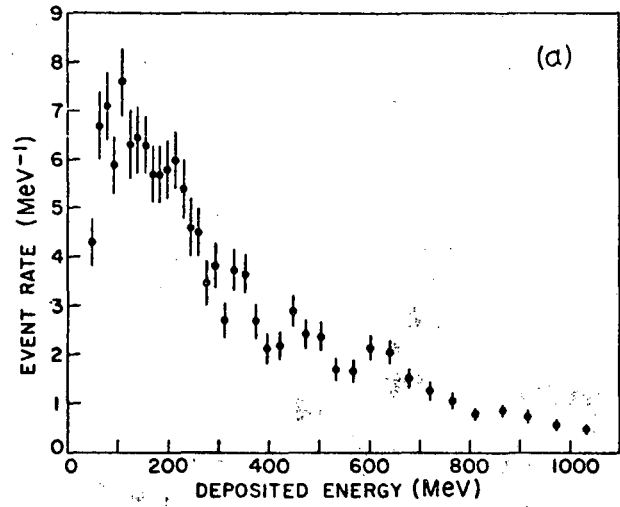


Fig. 32

XBL 7510-8478

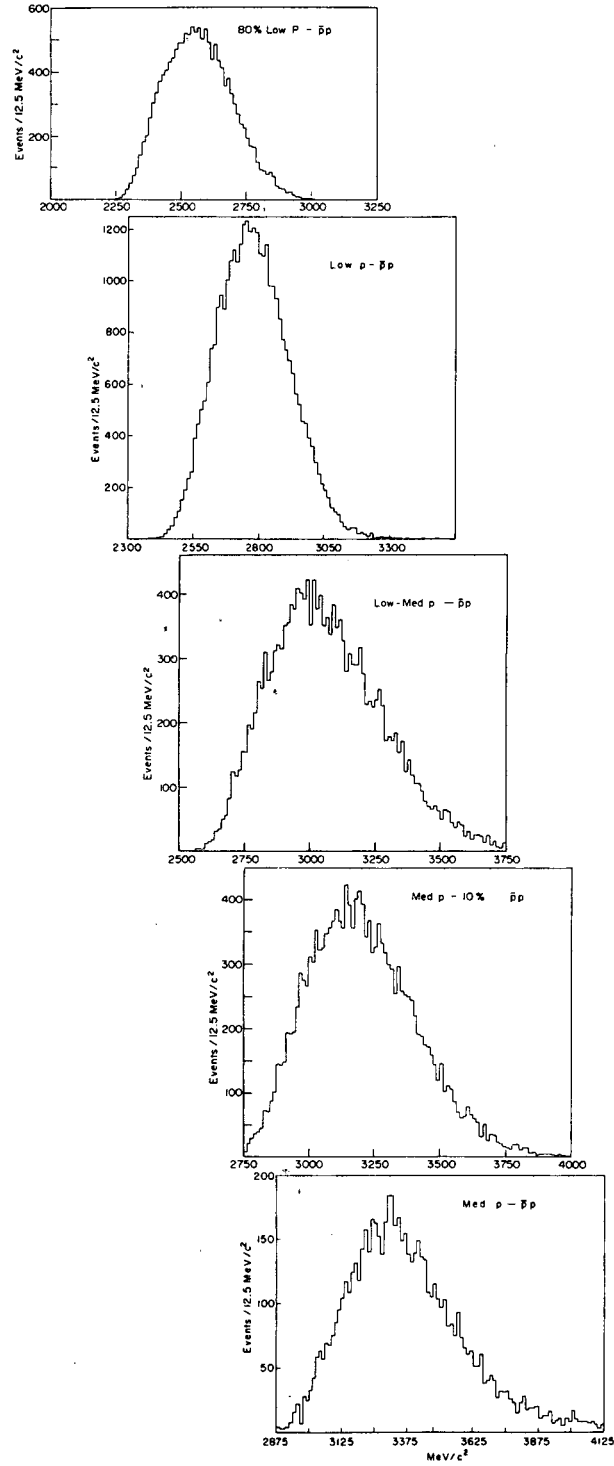


Fig. 33

XBL 7510-8479

000040209

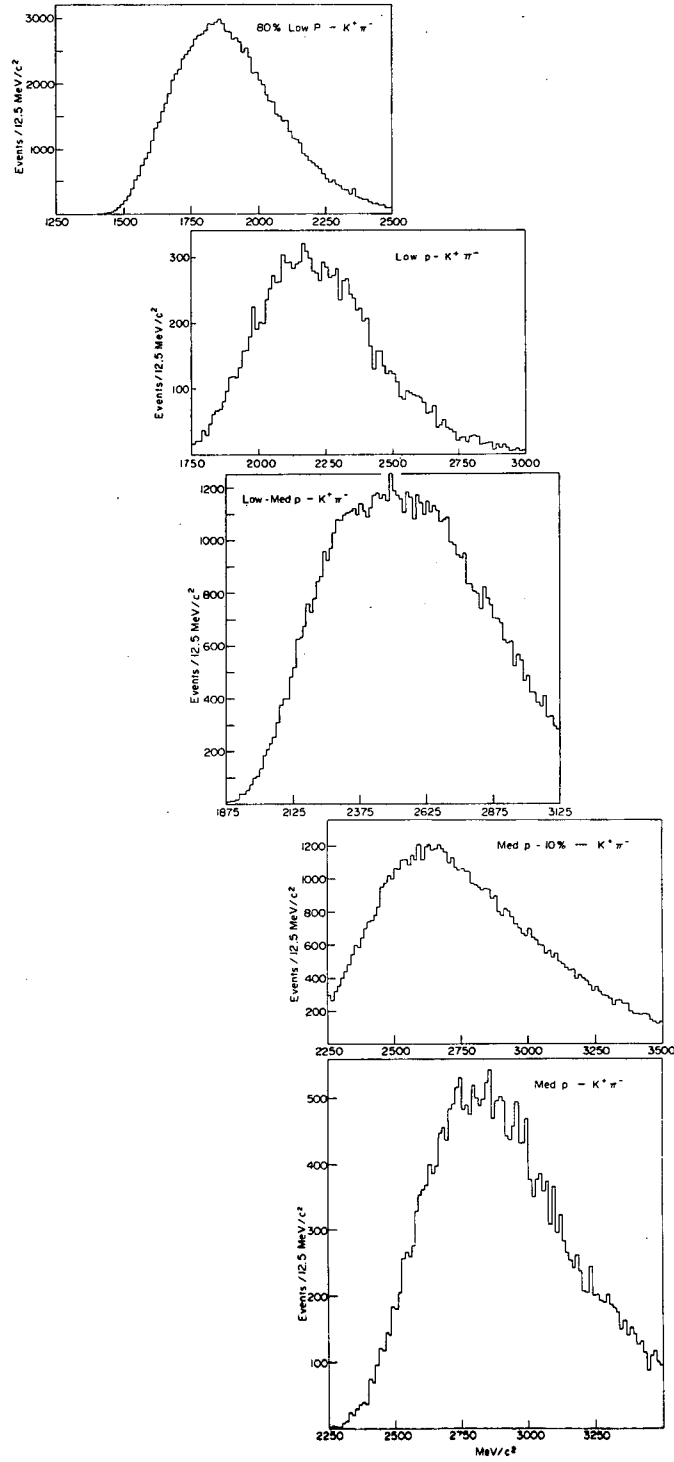


Fig. 34

XBL 7510-8480

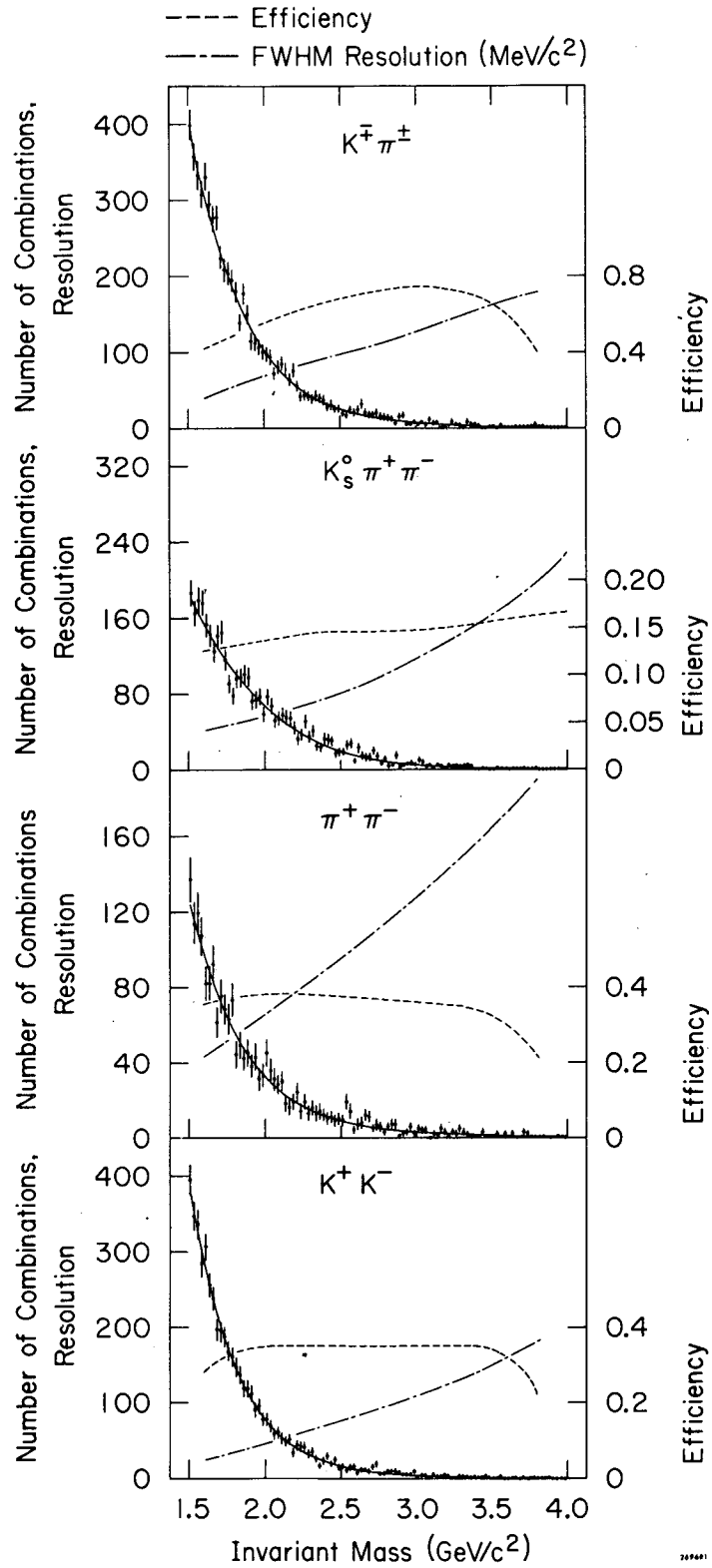


Fig. 35a

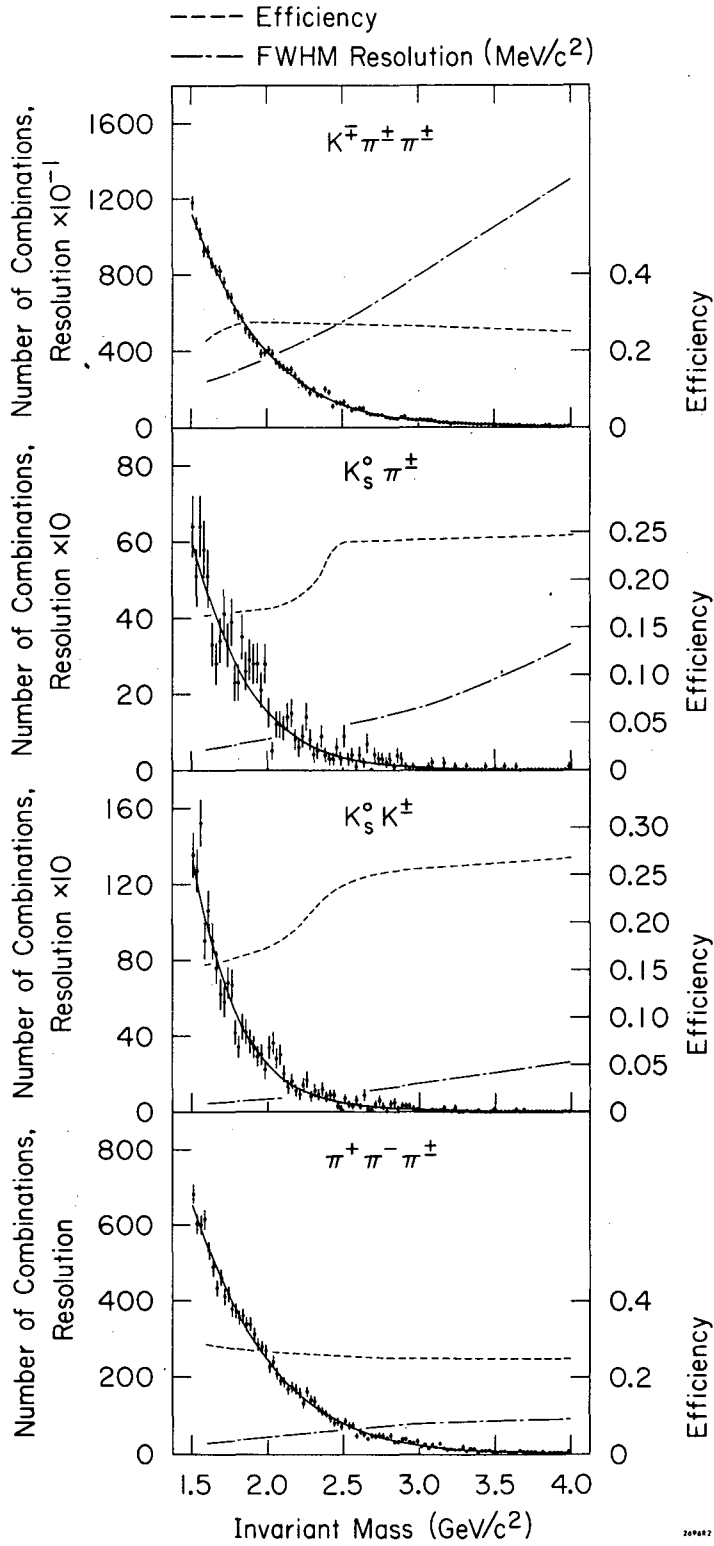


Fig. 35b

LEGAL NOTICE

This report was prepared as an account of work sponsored by the United States Government. Neither the United States nor the United States Energy Research and Development Administration, nor any of their employees, nor any of their contractors, subcontractors, or their employees, makes any warranty, express or implied, or assumes any legal liability or responsibility for the accuracy, completeness or usefulness of any information, apparatus, product or process disclosed, or represents that its use would not infringe privately owned rights.

0 1 9 7 0 7 4 0 0 0

TECHNICAL INFORMATION DIVISION
LAWRENCE BERKELEY LABORATORY
UNIVERSITY OF CALIFORNIA
BERKELEY, CALIFORNIA 94720